Hyperstretching in elongational flow of densely grafted comb and branch-on-branch model polystyrenes

Valerian Hirschberg ✉ iD ; Lorenz Faust; Mahdi Abbasi iD ; Qian Huang iD ; Manfred Wilhelm iD ;
Manfred H. Wagner iD

Check for updates

View Online Export Citation CrossMark

Hyperstretching in elongational flow of densely grafted comb and branch-on-branch model polystyrenes

Valerian Hirschberg,[1,a),b)] Lorenz Faust,[1] Mahdi Abbasi,[2] Qian Huang,[3] Manfred Wilhelm,[1,b)]
and Manfred H. Wagner[4,c)]

[1]*Institute of Chemical Technology and Polymer Chemistry (ITCP), Karlsruhe Institute of Technology (KIT),
Engesserstraße 18, 76131 Karlsruhe, Germany*
[2]*Borealis Polyolefine GmbH, Innovation Headquarters, 4021 Linz, Austria*
[3]*State Key Laboratory of Polymer Materials Engineering, Polymer Research Institute, Sichuan University,
610065 Chengdu, China*
[4]*Polymer Engineering / Polymer Physics, Berlin Institute of Technology (TU Berlin), Ernst-Reuter-Platz 1,
10587 Berlin, Germany*

Abstract

Strain hardening of long-chain branched polymers in elongational flow occurs due to the stretch of the backbone chain between branch points. With an increasing number of side arms, the length of the backbone chain segment between two branch points of a comb decreases. Of particular interest is the case when the number N_b of arms per entanglement length of the polymer is larger than one. This leads not only to larger strain hardening but also to hyperstretching, i.e., the elongational stress growth shows an enhanced increase with strain. We consider elongational data reported by Abbasi *et al.* [Macromolecules **50**(15), 5964–5977 (2017)] and Faust *et al.* [Macromol. Chem. Phys. **224**(1), 2200214 (2023)] on a series of comb and branch-on-branch polystyrene (PS) melts with the average number N_b of branches per entanglement segment of the backbone ranging from $N_b = 0.2$ to $N_b = 9.5$. In addition, we present measurements of the elongational viscosity of two PS combs with $N_b = 4.7$ as well as of blends consisting of 5 to 50 wt. % of a PS comb and a monodisperse linear PS. Analysis by the hierarchical multimode molecular stress function model shows that while backbone chains of loosely grafted combs with $N_b < 1$ are stretched affinely in elongational flow, backbone chains of more densely grafted combs with $N_b > 1$ show increasing hyperstretching with increasing N_b. The elongational data of the comb/linear blends confirm that hyperstretching is an intrinsic property of the comb macromolecule with $N_b > 1$, independent of its concentration in the blend. While this is of considerable interest from a modeling point of view, hyperstretching causing an enhanced increase of the elongational stress growth can also have a significant impact on the processability of polymers, and quantification of this effect is, therefore, important. © *2024 Author(s). All article content, except where otherwise noted, is licensed under a Creative Commons Attribution (CC BY) license (http://creativecommons.org/licenses/by/4.0/).*
https://doi.org/10.1122/8.0000781

I. INTRODUCTION

With the rapidly rising worldwide production of polymers and their waste [1], the need for a more sustainable use of polymeric materials also increases, and, therefore, enhanced processing properties and recyclability of polymers are of high importance. For processing of polymer melts, the optimization of strain hardening in extensional flows is a key goal. The rheological properties of homogeneous polymer melts are controlled especially by their molecular topology. By optimizing the topology of macromolecules, rheological properties beyond those of linear polymers can be obtained. Optimizing molecular topology allows creating new material properties and enables innovative applications and defined upcycling of polymers.

According to the tube model, chain stretching on the molecular level causes strain hardening in elongational flow [2,3]. Linear low-disperse polymers show rather weak strain hardening in elongational flow at strain rates $\dot{\varepsilon}$ above the inverse of the Rouse relaxation time τ_R, and no strain hardening can be observed at strain rates below the inverse of τ_R, i.e., at $\dot{\varepsilon} < 1/\tau_R$ [4,5]. Higher processing temperatures are very beneficial by reducing the shear viscosity, but high temperatures also reduce τ_R and, therefore, increase the minimum strain rate needed to initiate strain hardening of linear polymers. Consequently, polymers featuring strain hardening at high processing temperatures are extremely desirable. It is well-known that strain hardening can be induced by long-chain branching (LCB) [6,7]. The resistance of the branch points being pulled into the backbone tube increases the stress in the backbone, and so the chain segments between two branching points are stretched [8,9]. Consequently, in order to induce strain hardening via polymer topology in elongational flow, at least two branching points in the polymer molecule are needed, and the molecular design of branched polymers and the prediction of the resulting elongational properties are of considerable interest.

———————————

[a)]Also at: Institute for Technical Chemistry, Technical University Clausthal, Arnold-Sommerfeld-Str. 4, 38678, Clausthal-Zellerfeld, Germany
[b)]Authors to whom correspondence should be addressed; electronic mail: valerian.hirschberg@kit.edu and manfred.wagner@tu-berlin.de
[c)]Electronic mail: manfred.wagner@tu-berlin.de

In terms of polymer processing, the industrially most important branched polymer is low-density polyethylene (LDPE), which has an undefined comb and branch-on-branch structure and a strain hardening factor (SHF) typically around SHF = 10. By comparing commercial and experimental LDPEs, Stadler *et al.* [10] found that the SHF increases with the number of branches in the high-molecular-weight fraction. Well-defined branched model topologies investigated in the literature are star [11,12], comb [13–17], bottlebrush [18–20], H-shaped [21,22], pom-pom [23–26], and branch-on-branch topologies [27,28]. The rheological properties of blends are a nonlinear combination of the properties of the blend components [29], and, therefore, many blends of linear and branched polymers have been investigated [30–34].

Only a few systematic rheological investigations on the elongational rheology of polymer model systems with comb architecture are reported in the literature. Restricting attention to polystyrene (PS) combs, especially the works of Lentzakis and co-workers [14] as well as of Abbasi and co-workers [13] have to be mentioned. Lentzakis and co-workers focused on the impact of the molecular weight of the branches at a constant backbone molecular weight of $M_{w,bb}$ = 275 and 860 kg/mol, while keeping the number of branches per molecule in the range from 26 to 30. In contrast, Abbasi *et al.* investigated the impact of the number of branches from 3 up to 190 at a constant backbone molecular weight of $M_{w,bb}$ = 290 kg/mol and constant branch molecular weight of $M_{w,br}$ = 44 kg/mol. The average number N_b of branches per entanglement segment of the backbone varies from far less than one (N_b = 0.2) up to nearly 10 branches per entanglement (N_b = 9.5). As a consequence of the increasing number of branches, a transition of the linear-viscoelastic flow behavior from starlike for loosely grafted combs to the behavior of densely grafted combs and to bottlebrush combs was reported. In elongational flow, high strain hardening was observed and the SHF increases significantly with an increasing number of branches. Even higher strain hardening factors with SHF > 1000 were reported by Faust *et al.* [27] for three PS combs with the branch-on-branch topology.

The development of constitutive models based on molecular topology and their validation by comparison with rheological data of well-defined model systems are consequently of utmost importance. Based on the Doi--Edwards (DE) model [35,36], many constitutive models have been proposed to comprehend and predict the extensional rheology of polymers. While the original DE model is limited to linear polymers, later models like the pom-pom model [1] take into account the effect of LCB and assume that the chain segment between two branch points is stretched affinely up to a critical stretch, when the arms and their branch points are withdrawn into the tube of the backbone chain at sufficiently large deformations. Refinements of the pom-pom model are summarized, e.g., in [37]. However, for modeling of polydisperse LCB melts, at least two nonlinear fitting parameters per relaxation mode are needed, namely, a topological parameter and a stretch relaxation time. As pointed out in [38], this may be due to the preaveraging of the stretch in pom-pom models, which creates the need of a separate empirical stretch relaxation spectrum fitted to experimental data [37]. In

contrast, the molecular stress function (MSF) model [39] and further advanced models based on it such as the hierarchical multimode MSF (HMMSF) model [40–42], consider stretch as a relative quantity, i.e., stretch depends on the deformation of an entanglement segment between the time of its creation by diffusion and the time of stress observation. The HMMSF model is based on the concepts of hierarchical relaxation and dynamic dilution and features only one nonlinear material parameter in extensional flow, the dilution modulus. It was shown to be in agreement with the elongational rheology of a wide range of polydisperse linear and LCB polymers and also with two of the well-defined comb polymers investigated by Lentzakis and co-workers [40]. The ultimate aim of the HMMSF model is to fully predict strain hardening based solely on the linear-viscoelastic rheological characterization of the polymer melt by small amplitude oscillatory shear (SAOS) flow, which reflects the full impact of the topology of a polymer on its rheology. This was achieved recently for a series of model pom-pom PS melts with systematic variation of the molecular weight of the backbone as well as of the number and molecular weight of the branches [43]. The HMMSF model was found to be in quantitative agreement with the elongational rheology without any nonlinear material parameter, using only the spectrum of relaxation times and a dilution modulus, which for this series of pom-pom melts was equal to the plateau modulus. Another interesting research topic is brittle fracture at high strain rates in elongational flow [42,44–46], i.e., the elastic rupture of the polymer sample with a clear fracture surface. According to the entropic fracture criterion [46], brittle fracture occurs when the strain energy of a stretched entanglement segment exceeds the bond-dissociation energy of a single carbon–carbon bond.

The objective of this article is to investigate the impact of the number N_b of branches per entanglement segment on the stretch of the backbone of combs and combs with branch-on-branch side arms, and thereby on the strain hardening in elongational flow. In particular, we consider the case when there is more than one branch point per entanglement segment of the backbone, $N_b > 1$, and show that this leads to hyperstretching, i.e., the elongational stress growth coefficients $\eta_E^+(t)$ shows a stronger increase with time t and the elongational stress growth $\sigma_E^+(\varepsilon)$, an enhanced increase with the Hencky strain ε than expected for the affine stretch. Predictions of the HMMSF model are compared to experimental data of comb and branch-on-branch model polystyrenes as reported by Abbasi *et al.* [13] and Faust *et al.* [27]. In addition, we present measurements of the elongational stress growth coefficient of the combs PS310-100-15k and PS310-100-40k with a backbone molecular weight of $M_{w,bb}$ = 310 kg/mol and 100 branches of molecular weights of $M_{w,br}$ = 15 and 40 kg/mol, respectively, which corresponds to a branch density of N_b = 4.7 branches per entanglement of the backbone. We also investigated elongational viscosities of blends consisting of 5–50 wt. % of comb PS310-100-15k and a monodisperse linear polystyrene PS43k with M_w = 43 kg/mol. As we will show in the following, the HMMSF can quantitatively describe the tensile stress growth coefficient of the combs with $N_b < 1$ assuming the affine

stretch of the backbone. The only input parameters are the linear-viscoelastic relaxation spectrum and a single nonlinear parameter, the dilution modulus. At branching densities of $N_b > 1$, the analysis of the elongational stress growth data reveals a steeper increase of strain hardening with increasing Hencky strain than expected from the assumption of the affine stretch. This hyperstretching effect increases with increasing branching density and can well be predicted by implementing hyperstretching into the evolution equation of stretch. Additionally, with the blend series consisting of comb PS310k-100-15k and the linear PS43k, we confirm that hyperstretching is an intrinsic property of the comb macromolecule for $N_b > 1$, independent of its concentration in the blend.

II. HIERARCHICAL MULTIMODE MOLECULAR STRESS FUNCTION (HMMSF) MODEL WITH HYPERSTRETCHING

The HMMSF model is a generalized tube model with varying tube diameter, which takes hierarchical relaxation and dynamic dilution of tube segments into account as shortly summarized below. The extra stress tensor of the HMMSF model is given by [38,40,41],

$$\sigma(t) = \sum_i \int_{-\infty}^{t} \frac{\partial G_i(t - t')}{\partial t'} f_i^2(t, t') S_{DE}^{IA}(t, t') dt'. \quad (1)$$

The relaxation modulus $G(t)$ of the polymer melt is represented by discrete Maxwell modes with partial relaxation moduli g_i and relaxation times τ_i,

$$G(t) = \sum_i G_i(t) = \sum_i g_i \exp(t/\tau_i), \quad (2)$$

where S_{DE}^{IA} is the Doi and Edwards (DE) strain tensor assuming an independent alignment (IA) of tube segments, which is five times the second-order orientation tensor S,

$$S_{DE}^{IA}(t, t') \equiv 5 \left\langle \frac{\mathbf{u'u'}}{u'^2} \right\rangle_o = 5S(t, t'). \quad (3)$$

The bracket $\langle \cdots \rangle_o$ denotes an average over an isotropic distribution of unit vectors $\mathbf{u}(t')$ at time (t') and can be expressed as a surface integral over the unit sphere

$$\langle \cdots \rangle_o \equiv \frac{1}{4\pi} \oiint [\ldots] \sin \theta_o \, d\theta_o \, d\phi_o. \quad (4)$$

At the observation time t, the unit vectors are deformed to vectors $\mathbf{u}'$, which are calculated from the affine deformation hypothesis [with deformation gradient $\mathbf{F}^{-1}(t, t')$ being the relative deformation gradient tensor] as

$$\mathbf{u}'(t, t') = \mathbf{F}^{-1}(t, t') \bullet \mathbf{u}(t'), \quad (5)$$

where u' indicates the length of the vector $\mathbf{u}'$.

According to Doi and Edwards [see Eq. (A9) in [35]], the line density n/l, i.e., the number n of Kuhn segments (or statistically equivalent "monomer units") of length b that are found per length l of the tube, is a well-defined thermodynamic quantity and is given by $n/l = a/b^2$ with a being the tube diameter. If we apply this relation to a deformed tube segment of length l_i with diameter a_i containing n_i monomer units, the molecular stress functions $f_i = f_i(t, t')$ of Eq. (1) are given by

$$f_i(t, t') = \frac{l_i}{a_{i0}} = \frac{a_{i0}}{a_i(t, t')}, \quad (6)$$

with $a_{i0} = \sqrt{n_i b^2}$ being the equilibrium tube diameter. Thus, the molecular stress functions $f_i = f_i(t, t')$ are the inverse of the relative tube diameters a_i of each mode i and are functions of both the observation time t and the time t' of creation of entanglement segments by diffusion. According to Eq. (6), stretch is caused by a reduction of the tube diameter, i.e., by "tube squeeze." Neglecting stretch relaxation, the molecular stress functions $f_i = f_i(t, t')$ can be derived from an evolution equation

$$\frac{\partial f_i}{\partial t} = f_i(\mathbf{K} : \mathbf{S}), \quad (7)$$

where k is the velocity gradient and for simplicity, we have dropped the dependence on (t, t'). Equation (7) has the analytical solution [39]

$$f_i = \exp[\langle \ln(u') \rangle_0] \approx \langle u' \rangle_0, \quad (8)$$

which reflects an affine stretch of entanglement segments characterized by the average of the length of deformed unit vectors according to Eq. (5). From Eqs. (6) and (8) follows that the normalized tube segment volume v_i reduces with deformation according to

$$v_i = f_i(a_i/a_{i0})^2 = \exp[-\langle \ln(u') \rangle_0] \approx \langle u' \rangle_0^{-1}. \quad (9)$$

i.e., inversely proportional to the average stretch $\langle u' \rangle_0$, while affine stretch and reduction of the tube segment volume were found to be in agreement with the rheology of linear and randomly long-chain branched (LCB) polymers [41,42] as well as for model Pom-Pom PS [38], a different approach may be appropriate for the case of combs with densely grafted side chains, if there is more than one side chain per entanglement segment of the backbone, i.e., if $N_b > 1$. In loosely grafted combs with $N_b < 1$, branch points and entanglements pin the backbone chain to the deforming continuum of the surrounding chains, which results in affine stretch of the entanglement segments of the backbone. As far as stretching is concerned, there is no difference between branch points and entanglements (when viewed as localized topological constraints, e.g., in the form of slip links), except that branch points restrain chain retraction. However, in the case of densely grafted combs with $N_b > 1$, there are several branch points per entanglement segment of the backbone, causing

additional topological constraints on length scales smaller than the entanglement length and therefore creating extra tension. We assume that this extra tension can be expressed by a higher exponent scaling between molecular stress function f_i and inverse relative tube diameter a_{i0}/a_i,

$$f_i = \left(\frac{a_{i0}}{a_i}\right)^{1+k} = \exp\left[(1+k)\langle\ln(u')_0\rangle\right] \approx \langle u'\rangle_0^{1+k}, \quad (10)$$

where we have introduced the hyperstretch factor k with $k > 0$ for $N_b > 1$, and $k = 0$ for $N_b < 1$. The normalized tube segment volume v_i is then given by

$$v_i = f_i(a_i/a_{i0})^2 = \exp\left[(k-1)\langle\ln(u')\rangle_0\right] \approx \langle u'\rangle_0^{k-1}. \quad (11)$$

For the case of $k = 1$, the normalized tube segment volume is $v_i = 1$, i.e., due to hyperstretching the volume of the entanglement segment does not change with deformation but remains constant. From Eq. (10), the stretch increases then according to $\langle u'\rangle_0^2$, which we may consider tentatively as maximal hyperstretching. From Eq. (10), the evolution equations of the molecular stress functions f_i are given by

$$\frac{\partial f_i}{\partial t} = (1+k)f_i(\mathbf{K}:\mathbf{S}). \quad (12)$$

Restricting attention to comb polymers in extensional flows and accounting for the effects of stretch relaxation [43], which in the case of LCB polymers depends on the relaxation times τ_i and not the Rouse time of the chain, the evolution equation for the molecular stress function f_i of each mode i can be expressed as

$$\frac{\partial f_i}{\partial t} = (1+k)f_i(\mathbf{K}:\mathbf{S}) - \frac{f_i-1}{\tau_i}(1-w_i^2) - \frac{(f_i^5-1)}{5\tau_i}w_i^2, \quad (13)$$

with the initial conditions $f_i(t = t', t') = 1$. The first term on the right-hand side represents the hyperstretching rate, the second term takes into account stretch relaxation, and the third term limits stretch due to enhanced relaxation of stretch on smaller length scales as shown in [47], leading to a stretch relaxation term that is proportional to the 5th power of the stretch f_i.

The stretch relaxation terms of Eq. (13) depend on the weight fractions w_i of the relaxation modes, and account for hierarchical relaxation and dynamic dilution because chain segments with shorter relaxation times dilute those with longer relaxation times. The weight fractions w_i are derived from the linear-viscoelastic spectrum by distinguishing two dilution regimes during the relaxation process, namely, "permanent" dilution and "dynamic" dilution. Permanent dilution is caused by oligomeric chains and unentangled/fluctuating chain ends. Dynamic dilution starts when the relaxation modulus $G(t)$ at time $t = \tau_D$ has reached the dilution modulus $G_D \le G_N^0$, which is a free parameter of the model and which is fitted to nonlinear viscoelastic experimental data, since the fraction of oligomeric chains and fluctuating chain ends is often not known. Chain segments, which

relaxed at times $t \le \tau_D$, are assumed to be permanently diluted. The weight fraction w_i of dynamically diluted linear or LCB polymer segments with relaxation time $\tau_i > \tau_D$ is determined by the ratio of the relaxation modulus at time $t = \tau_i$ to the dilution modulus G_D,

$$w_i^2 = \frac{G(t=\tau_i)}{G_D} = \frac{1}{G_D}\sum_{j=1}^{n} g_j\exp(-\tau_i/\tau_j) \quad \text{for } \tau_i > \tau_D,$$
$$w_i^2 = 1 \qquad\qquad \text{for } \tau_i \le \tau_D. \quad (14)$$

The value of w_i obtained at $t = \tau_i$ is attributed to the chain segments with relaxation time τ_i. Segments with $\tau_i < \tau_D$ are considered to be permanently diluted, i.e., their weight fractions are fixed at $w_i = 1$. As shown by Narimissa *et al.* [48], these assumptions allow modeling the rheology of broadly distributed polymers, largely independent of the number of discrete Maxwell modes used to represent the relaxation modulus $G(t)$.

Thus, the HMMSF model for LCB polymer melts consists of multimode stress Eq. (1), a set of evolution equations for the molecular stresses f_i, Eq. (13), and a hierarchical procedure to quantify the fraction of dynamically diluted chain segments according to Eq. (14) with two free nonlinear parameters, the dilution modulus G_D and the hyperstretch factor k. Once the linear-viscoelastic relaxation spectrum of a polydisperse polymer melt is known, the weight fractions w_i in the evolution of Eq. (13) can be obtained by fitting the value of G_D to the elongational viscosity. The parameter G_D, in conjunction with the hyperstretch factor k, determines the extent of strain hardening. These two free parameters are sufficient for modeling extensional flows of comb polymers.

We add a note on finite extensible nonlinear elasticity (FENE) here: As explained in [42], due to dilution of the backbone chain by side chains, FENE effects can be neglected as long as deformation rates are sufficiently small so that side chains are not stretched. Also, FENE effects are expected to be of significance at large strains, while the effect of hyperstretching is already affecting the start-up stress growth as soon as stretching begins (see Figs. 9 and 11). Thus, the effect of hyperstretching is fundamentally different from the effect of FENE. We also note that "affine stretch" is not equivalent to "affine deformation" as implemented in the multimode Oldroyed B model or its integral version, the Lodge rubberlike equation [4,38]

$$\sigma(t) = \int_{-\infty}^{t} \frac{\partial G(t-t')}{\partial t'}\mathbf{C}^{-1}(t, t')dt', \quad (15)$$

with $\mathbf{C}^{-1} = \mathbf{F}^{-1}(\mathbf{F}^T)^{-1} = 3\langle\mathbf{u}'\mathbf{u}'\rangle_0$ being the relative Finger strain tensor. While affine deformation assumes that the end-to-end vectors of entanglement segments are deformed as prescribed by the macroscopic deformation of the material, constitutive models of the type of Eq. (1) and its preaveraged approximations [38] distinguish between the effects of chain orientation and chain stretch.

In elongational flow of polymer samples showing strong transient strain hardening, brittle, or elastic fracture at higher strain rates is frequently observed [44,45]. According to the entropic fracture hypothesis [42,43,46], a fracture will occur when the strain energy of a chain segment reaches the bond energy U of a carbon–carbon bond. Due to thermal fluctuations, the total strain energy of the chain segment will be concentrated on one C–C bond by thermal fluctuations and the bond ruptures. This leads to crack initiation and within a few milliseconds to macroscopic fracture. The critical stretch $f_{i,c}$ at fracture is given by

$$f_{i,c} = \sqrt{\frac{U}{3kT}\frac{1}{w_i}}, \qquad (16)$$

with k being the Boltzmann constant and T the absolute temperature. The ratio of bond-dissociation energy U to thermal energy $3kT$ is approximately $U/3kT = 32$ and 31 at temperatures of $T = 160$ and $180\,°C$, respectively. This fracture criterion has been shown to be in agreement with experimental evidence of polymer melts and solutions, see, e.g., [32,42,43,46,47].

III. MATERIALS AND EXPERIMENTAL DATA

The linear PS was synthesized by living anionic polymerization, and the comb PS by a combination of living anionic polymerization and grafting as shown schematically in Fig. 1. PS anions ($M_{w,a} = 15$ and $44\,kg/mol$) as arms were grafted onto a postfunctionalized PS backbone ($M_{w,bb} = 290$ and $310\,kg/mol$), yielding the long-chain branched comb topology. In more detail, first, a linear PS was synthesized by anionic polymerization (a) and then postfunctionalized via a Friedel−Crafts acylation (b). In a third step (c), the arms were prepared by anionic polymerization and (d) added to the postfunctionalized backbone from step (b), so that they were grafted onto it. A more detailed explanation of this synthesis route and the molecular characterization with SEC-MALLS and NMR of the obtained comb model systems can be found in [13,49].

The molecular characteristics of the comb model systems are shown schematically in Fig. 2(b) and are summarized in Table I, listing $M_{w,bb}$, the branch number Nbr, the number of branched per entanglement segment of the backbone N_b, the molecular weight of the branches $M_{w,br}$, the total molecular weight M_w, and the dispersity of the comb D_t. The number of branches per entanglement segment of the backbone is given by $N_b = Nbr/z_{bb}$. The number of entanglement segments of the backbone is $z_{bb} = M_{w,bb}/M_e$, with the entanglement molecular weight taken as $M_e = 14.5\,kg/mol$ [13]. N_b ranges from 0.2 up to 9.5. Plateau modulus G_N^0 and zero-shear viscosity η_0 of the PS combs at $T = 180\,°C$ are summarized in Table II.

The branch-on-branch PS was synthesized similar to the comb PS by a combination of living anionic polymerization and grafting as shown schematically in Fig. 2(a), using a long-chain branched comb as the precursor instead of a linear PS as for the combs. PS anions ($M_{w,br,BoB} = 14\,kg/mol$) as BoB arms were grafted onto a postfunctionalized comb PS as the precursor, yielding the branch-on-branch topology. Therefore, first a comb PS was synthesized as described in Fig. 1, and then again postfunctionalized via a Friedel−Crafts acylation (1). In the next step (2), the arms were prepared by anionic polymerization and (3) added to the postfunctionalized comb precursor from step (1) so that they were grafted onto it. A more detailed explanation of this
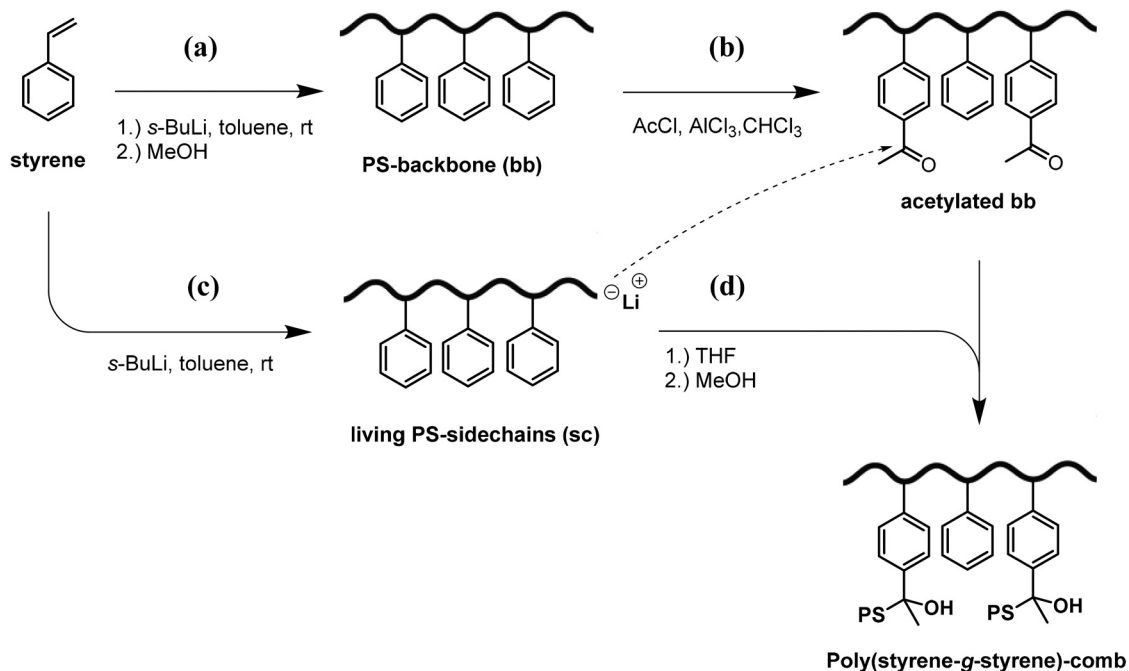
FIG. 1. Reaction scheme for the synthesis of model PS combs with the four steps: (a) Anionic polymerization of the backbone. (b) Postfunctionalization of the backbone by Friedel−Crafts acylation. (c) Anionic polymerization of the living side chains. (d) Grafting of the PS anions as side chains onto the acetylated backbone.
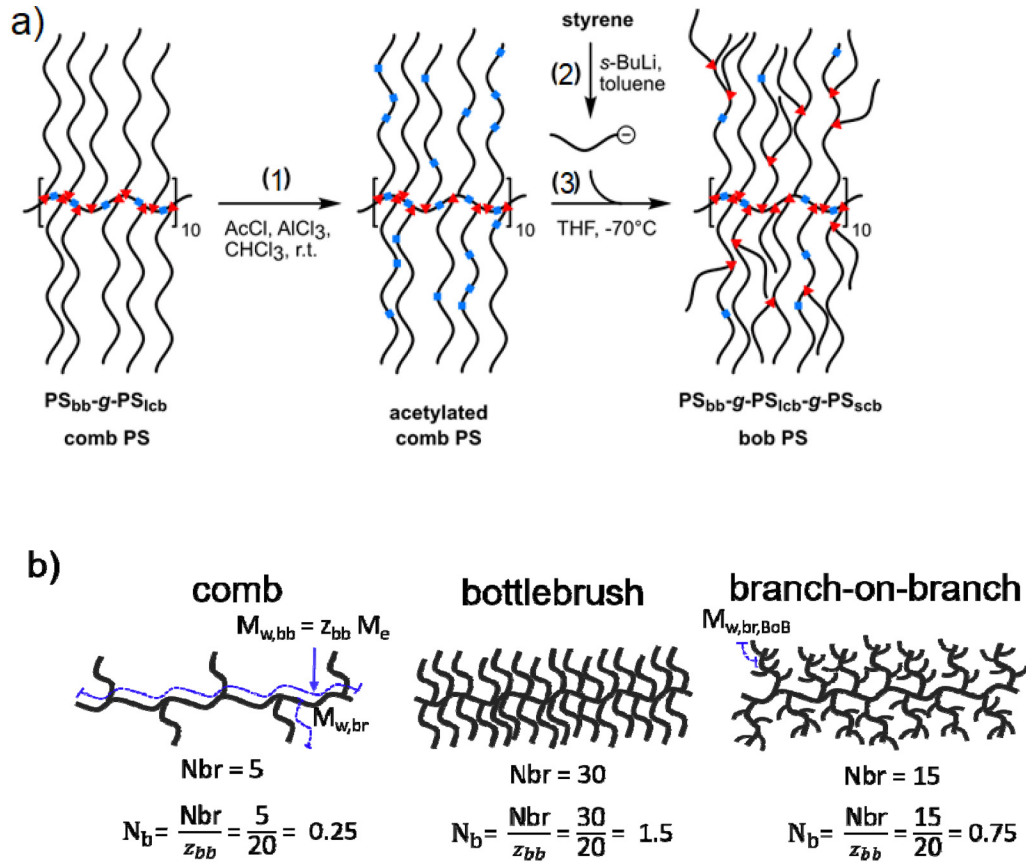
FIG. 2. (a) Reaction scheme for the synthesis of model branch-on-branch (BoB) PS using a long-chain branched comb PS as the precursor. (1) Functionalization of the LCB comb PS310-100-40 by adding carbonyl functional groups (■) via Friedel–Crafts acylation, similar to the comb synthesis shown in Fig. 1. (2) Anionic polymerization of living arms with $M_{w,br,BoB} \approx 14$ kg/mol. (3) Grafting of the BoB arms onto the acetylated comb precursor. The carbonyl groups turn into branch points (▲). (b) Schematic of polymer topologies considered: From comb to bottlebrush to branch-on-branch.

synthesis route and the molecular characterization with SEC-MALLS and NMR of the obtained BoB model systems can be found in [27]. The molecular characteristics of the BoB model systems are shown schematically in Fig. 2(b) and are summarized in Table III, and plateau modulus G_N^0 and zero-shear viscosity η_0 at T = 180 °C are given in Table IV.

The linear PS used for blending with PS310-100-15k has a molecular weight of $M_w = 43$ kg/mol and a dispersity of Đ = 1.04 and was used before as a blend component in [43].

The blends were made by a four-step solvent blending procedure similar to the one described in the literature [43,50]. First, linear and comb PSs were both dissolved in tetrahydrofuran (THF) at room temperature and stirred overnight, followed by slow evaporation, and, finally, drying under vacuum for 24 h at 40 °C and a final 2 h drying at 115 °C, slightly above the glass transition temperature (T_g) of PS to remove the last remaining traces of THF. A summary about the weight content of the comb in the linear PS43k and the rheological properties of the comb/linear blends is given in Table V.

TABLE I. Molecular characteristics of investigated PS combs, assuming $M_e = 14.5$ kg/mol.

Comb	$M_{w,bb}$ (kg/mol)	Nbr (—)	N_b (—)	$M_{w,br}$ (kg/mol)	M_w (kg/mol)	D_t (—)
PS290k	290	—	—	—	290	1.10
PS290k-3-44k	290	3	0.2	45	420	1.11
PS290k-10-44k	290	10.4	0.5	44	750	1.15
PS290k-14-44k	290	13.8	0.7	45	900	1.08
PS290k-30-44k	290	29.8	1.6	43	1600	1.03
PS290k-60-44k	290	59.5	3.0	44	2900	1.03
PS290k-120-44k	290	120	6.0	44	5570	1.11
PS290k-190-44k	290	189.3	9.5	44	8620	1.07
PS310k-100-40k	310	100	4.7	40	4200	1.13
PS310k-100-15k	310	100	4.7	15	1810	1.33

TABLE II. Zero-shear viscosity η_0, plateau modulus G_N^0, dilution modulus G_D, number N_b of branches per entanglement segment of the backbone, and hyperstretch factor k of PS combs at T = 180 °C.

Comb	η_0(kPa s)	G_N^0(kPa)	G_D(kPa)	N_b (—)	k (—)
PS290k-3-44k	344	200	5	0.2	0
PS290k-10-44k	1920	220	5	0.5	0
PS290k-14-44k	751	210	80	0.7	0
PS290k-30-44k	241	250	250	1.6	0.2
PS290k-60-44k	89	210	210	3.0	0.5
PS290k-120-44k	170	250	250	6.0	0.6
PS290k-190-44k	5750	190	190	9.5	1

TABLE III. Molecular characteristics of the branch-on-branch (BoB) PS having the same long-chain branched comb precursor with $M_{w,br} \sim 40$ kg/mol as a first generation and then 123, 236, and 461 short arms of $M_{w,br,BoB} \sim 14$ kg/mol grafted onto the first generation, respectively.

BoB	$M_{w,bb}$ (kg/mol)	Nbr (—)	N_b (—)	$M_{w,br}$ (kg/mol)	N_{BoB} (—)	$M_{w,br,BoB}$ (kg/mol)	M_w (kg/mol)	D_t (—)
PS310k-100-40k-g-120-14 k	310	98	4.7	39	123	14	5 900	1.10
PS310k-100-40k-g-240-14 k	310	98	4.7	39	236	14	7 600	1.11
PS310k-100-40k-g-460-14 k	310	98	4.7	39	461	13	10 100	1.15

The experimental protocol for the rheological measurements in shear and elongation with the extensional viscosity fixture (EVF) is reported in [13]. In addition to the elongational viscosity data of Abbasi *et al.* [13], we present elongational viscosity measurements using a filament stretching rheometer (FSR) [51] for several systems of the PS290-Nbr-44k comb series. The FSR measurement data are indicated in Figs. 5–8 by red symbols. Except at low strain rates, a good agreement between the elongational data obtained by EVF and FSR is observed, which supports the validity of the data set. For PS310-100-15k and its blends, the oscillatory shear and uniaxial extensional rheology were conducted on an ARES-G2 rheometer (TA Instruments, Newcastle, USA) using a 13 mm plate–plate geometry for the shear measurements as well as an EVF for uniaxial elongational tests. The dried blends were hot-pressed at 180 °C for 10 min under vacuum. Shear rheology was measured between 130 and 220 °C, using an angular frequency range of $\omega = 0.1$ to 100 rad/s. The elongational tests were performed at 160 or 180 °C, at Hencky strain rates of $\dot{\varepsilon} = 0.003$ to $10\,\mathrm{s}^{-1}$ with a maximum Hencky strain of $\varepsilon = 4$ for the EVF. The FSR extensional experiments were performed at 180 °C and at low and medium strain rates up to $\varepsilon = 7$ or up to the breakage of the samples.

For all samples investigated, linear-viscoelastic master curves of storage and loss modulus, G' and G'' were obtained by time-temperature superposition (TTS) and are shown in Figs. SI.1–SI.9 of the supplementary) material [54]. The TTS factors are given in Tables SI.1–SI.3. The mastercurves were fitted by parsimonious relaxation spectra by the IRIS software [52,53] and are also summarized in the SI. The plateau modulus G_N^0 is taken as the value of the storage modulus G' at the high frequency G' minimum of the loss tangent δ. In a few specific cases such as for comb PS290k-190-44k (Fig. SI.7) and the BoB polymers [Figs. SI.8(b)–SI(d)], the terminal regime has not been reached. However, the linear-viscoelastic master curves of storage and loss

modulus extend down to frequencies of 10^{-4} rad/s or lower, and thus the experimental window of the elongational stress growth coefficients $\eta_E^+(t)$ measured at elongation rates of $\dot{\varepsilon} \geq 0.01\,\mathrm{s}^{-1}$ was sufficiently covered by the truncated relaxation spectra.

IV. COMPARISON OF ELONGATIONAL VISCOSITY DATA OF COMBS TO MODEL PREDICTIONS

Figures 3 and 4 compare the experimental data (symbols) of the elongational stress growth coefficient $\eta_E^+(t)$ as a function of time t and the elongational stress $\sigma_E^+(\varepsilon)$ as a function of Hencky strain ε for the loosely grafted combs PS290-3-44k and PS290k-10-44k with 3 and 10 branches corresponding to $N_b = 0.2$ and $N_b = 0.5$ branches per entanglement segment, respectively. Agreement of the $\eta_E^+(t)$ as well as $\sigma_E^+(\varepsilon)$ data is obtained with predictions (lines) of the HMMSF model for a dilution modulus of $G_D = 5.0 \times 10^3$ Pa and without assuming hyperstretching, i.e., $k = 0$ for both comb systems. This is in agreement with earlier results for randomly branched LCB polymers [41].

Again, without hyperstretching, i.e., $k = 0$, the elongational data of comb PS290k-14-44k (Fig. 5) can be quantitatively described by the HMMSF model. Due to the higher number of branches, dynamic dilution is more pronounced and a dilution modulus of $G_D = 8.0 \times 10^4$ Pa is found to be in agreement with the experimental data. With 14 branches, PS290k-14-44k has $N_b = 0.7$ branches per entanglement segment of the backbone and is, therefore, in the regime of $N_b < 1$.

In addition to the elongational data (black symbols) obtained by the EVF, Figs. 5–8 show measurements with a FSR at medium and low strain rates and indicated by data symbols in red. Within experimental accuracy, agreement between measurements with EVF and FSR is found at the

TABLE V. Pom-pom/linear PS blends of comb PS310-100-15k and linear PS43k. φ indicates the weight percent of the PS comb in the blends. Zero-shear viscosity η_0, plateau modulus G_N^0, dilution modulus G_D, number N_b of branches per entanglement segment of the backbone, and hyperstretch factor k at 160 °C.

$\phi_{PS310k-100-15k}$ (wt. %)	η_0 (kPa s)	G_N^0 (kPa)	G_D (kPa)	N_b (—)	k (—)
100	550	320	320	4.7	0.6
50	66	180	180	4.7	0.6
20	16	200	200	4.7	0.6
10	5.0	160	160	4.7	0.6
5	4.8	200	200	4.7	0.6
PS43k	3.0	—	—	—	—

TABLE IV. Zero-shear viscosity η_0, plateau modulus G_N^0, dilution modulus G_D, number N_b of branches per entanglement segment of the backbone, and hyperstretch factor k of BoB polymers and precursors at T = 180 °C.

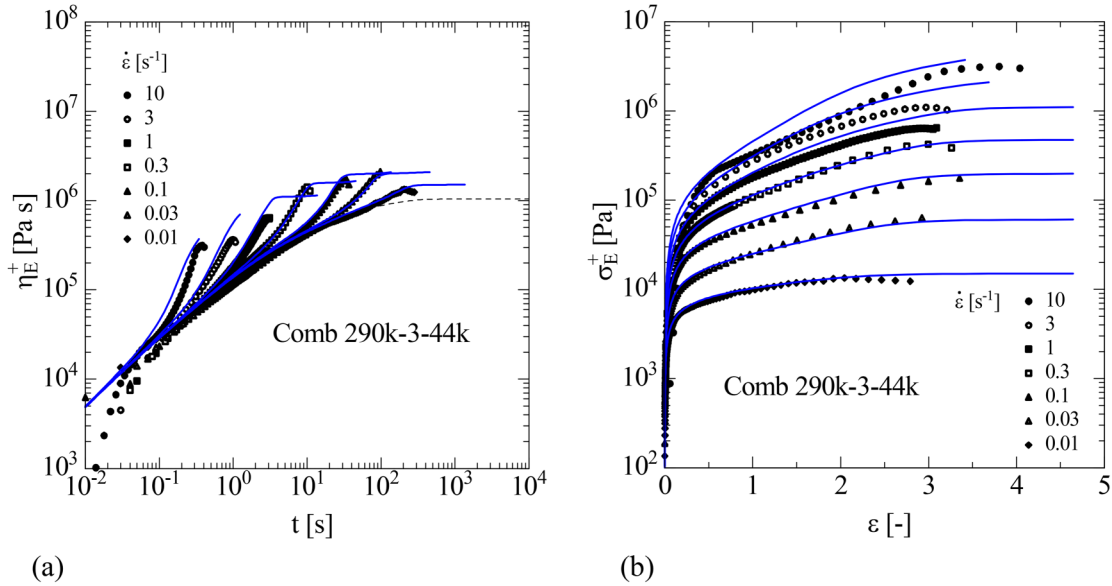| Comb/BoB	η_0 (kPa s)	G_N^0 (kPa)	G_D (kPa)	N_b (—)	k (—)
PS310-100-40k	139	220	220	4.7	0.6
PS310-100-40k-g-120-14k	536	220	220	4.7	1
PS310-100-40k-g-240-14k	711	250	250	4.7	1
PS310-100-40k-g-460-13k	896	270	270	4.7	1

FIG. 3. Experimental data (symbols) of (a) elongational stress growth coefficient $\eta_E^+(t)$ as a function of time t, and (b) elongational stress $\sigma_E^+(\varepsilon)$ as a function of Hencky strain ε for the comb PS290k-3-44k at T = 180 °C. Lines are predictions of the HMMSF model with $G_D = 5.0 \times 10^3$ Pa and $k = 0$.

medium strain rates, while some deviations are seen at the lowest strain rates due to possible sagging of the samples at small elongational stresses and long measurement times. We note that the measuring principles of EVF and FSR differ significantly with EVF relying on global sample deformation versus FSR focusing on local deformation, and, therefore, the general agreement of EVF and FSR measurements is encouraging and supports the validity of the uniaxial extensional data presented. The measurements by FSR extend to larger Hencky strains and confirm the approach to a steady-state elongational stress at lower strain rates, while filament fracture occurs at higher strain rates, in general agreement with the entropic fracture criterion of Eq. (16). The approach to a steady state is seen in the $\sigma_E^+(\varepsilon)$ plots of Figs. 6 and 7, which

also show that the apparent overshoot of the elongational stress growth coefficient $\eta_E^+(t)$ is likely due to loss of sample homogeneity at very high strains.

A first indication of hyperstretching is revealed by close inspection of the elongational flow data of comb PS290k-30-44k (Fig. 6) with 30 branches. Hyperstretching is hardly discernible by examining the elongational stress growth coefficient $\eta_E^+(t)$ in Fig. 6(a), where experimental data are in reasonable agreement with HMMSF predictions using the affine stretch assumption with $k = 0$. However, the elongational stress growth $\sigma_E^+(\varepsilon)$ is slightly underpredicted by the HMMSF model with $k = 0$. Substantially improved agreement between experimental data and predictions of both $\eta_E^+(t)$ and $\sigma_E^+(\varepsilon)$ can be obtained by use of a hyperstretch
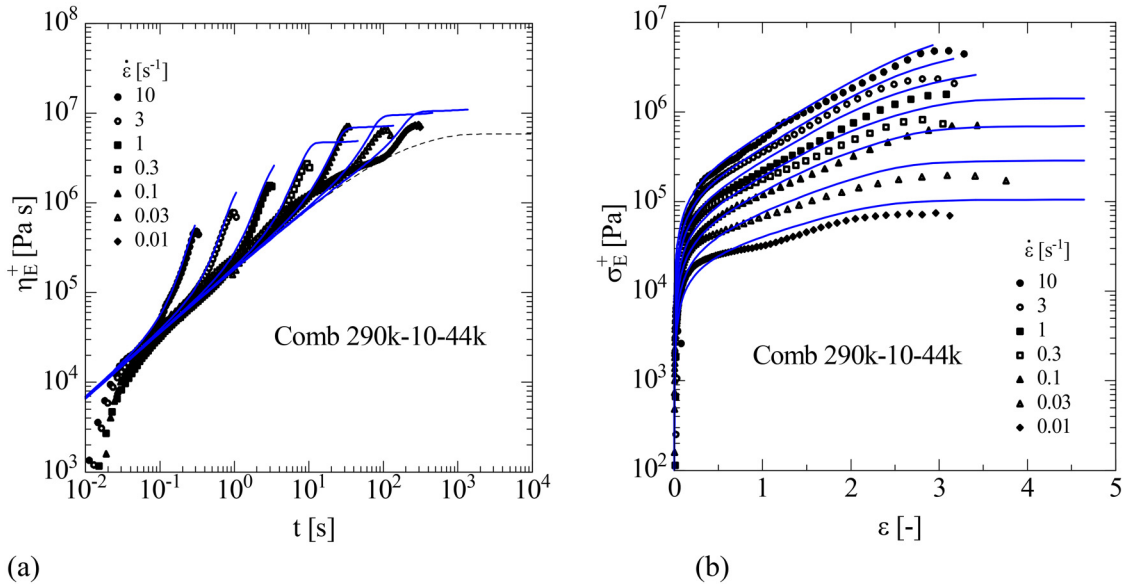
FIG. 4. Experimental data (symbols) of (a) elongational stress growth coefficient $\eta_E^+(t)$ as a function of time t and (b) elongational stress $\sigma_E^+(\varepsilon)$ as a function of Hencky strain ε for the comb PS290k-10-44k at T = 180 °C. Lines are predictions of the HMMSF model with $G_D = 5.0 \times 10^3$ Pa and $k = 0$.
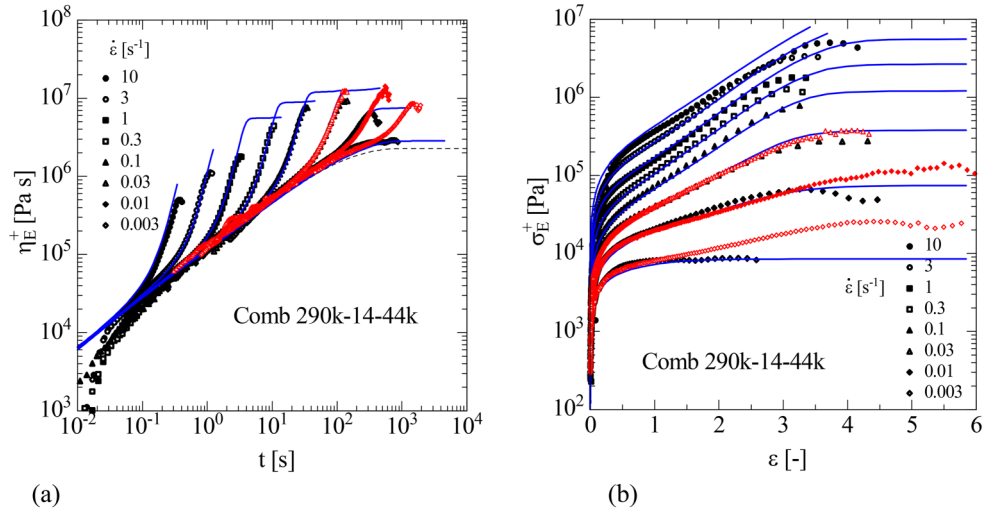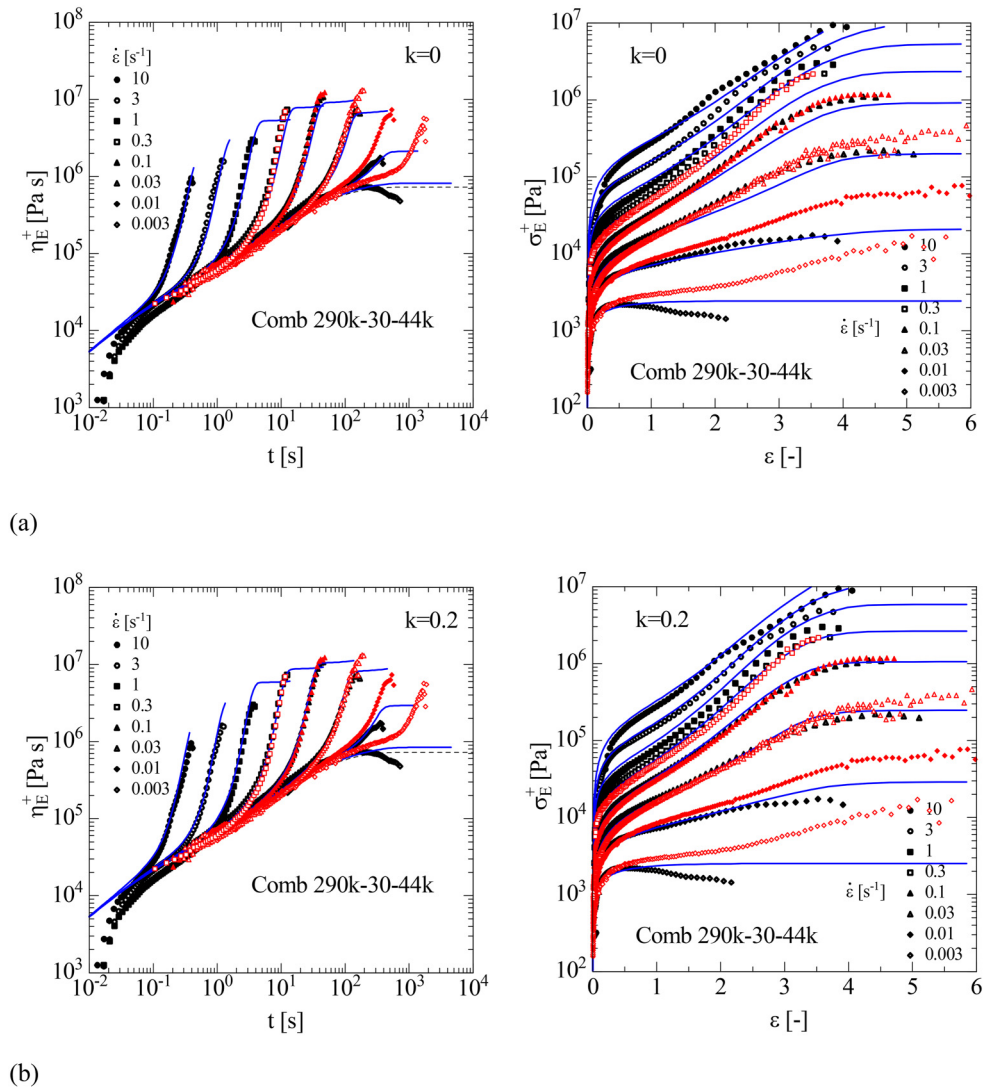
FIG. 5. Experimental data measured with EVF and FSR (black and more crowded symbols) of (a) elongational stress growth coefficient $\eta_E^+(t)$ as a function of time t and (b) elongational stress $\sigma_E^+(\varepsilon)$ as a function of Hencky strain ε for the comb PS290k-14-44k at T = 180 °C. Lines are predictions of the HMMSF model with $G_D = 8.0 \times 10^4$ Pa and $k = 0$.

FIG. 6. Experimental data measured with EVF and FSR (black and more crowded symbols) of elongational stress growth coefficient $\eta_E^+(t)$ as a function of time t and elongational stress $\sigma_E^+(\varepsilon)$ as a function of Hencky strain ε for the comb PS290k-30-44k at T = 180 °C. Lines are predictions of the HMMSF model with $G_D = G_N^0 = 2.5 \times 10^5$ Pa and $k = 0$ (a), and $k = 0.2$ (b), respectively.
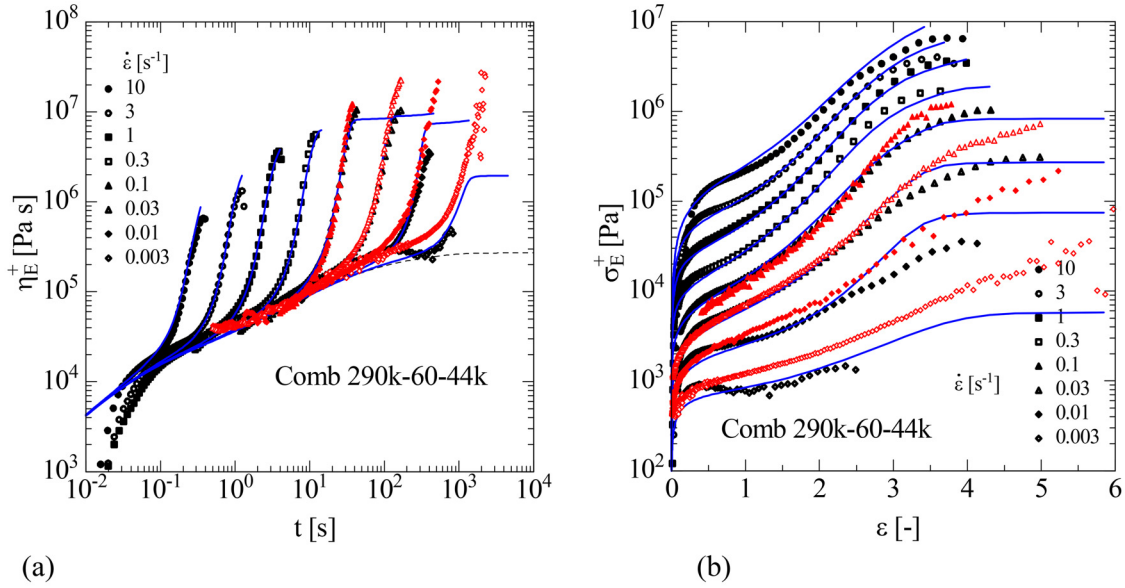
FIG. 7. Experimental data measured with EVF and FSR (black and more crowded symbols) of (a) elongational stress growth coefficient $\eta_E^+(t)$ as a function of time t and (b) elongational stress $\sigma_E^+(\varepsilon)$ as a function of Hencky strain ε for the comb PS290k-60-44k at T = 180 °C. Lines are predictions of the HMMSF model with $G_D = G_N^0 = 2.1 \times 10^5$ Pa and $k = 0.5$.

factor of $k = 0.2$ [Fig. 6(b)]. Comb PS290k-30-44k has, on average, $N_b = 1.6$ branches per entanglement length of the backbone, and we conclude that hyperstretching occurs as soon as the number N_b of branches per backbone entanglement is larger than one, i.e., $N_b > 1$.

We also note that for all combs PS290k-Nbr-44k with Nbr > 30 investigated, the dilution modulus G_D is identical to the plateau modulus G_N^0 (Table II), i.e., dynamic dilution of the backbone according to Eq. (14) starts as soon as the relaxation modulus $G(t)$ has reached the value of the plateau modulus. For combs PS290k-60-44k with 60 branches and $N_b = 3$ (Fig. 7) and PS290k-120-44k with 120 branches and

$N_b = 6$ (Fig. 8), agreement between experimental data and HMMSF model predictions is obtained by the use of hyperstretch factors of $k = 0.5$ and $k = 0.6$, respectively. Deviations are only seen at the lowest strain rates, where also EVF and FSR measurements deviate. For PS290k-120-44k, the effect of hyperstretching on the elongational stress growth coefficient $\eta_E^+(t)$ is demonstrated by comparing predictions of the HMMSF model with $k = 0$ [Fig. 8(a)] to predictions with $k = 0.6$ [Fig. 8(b)]. Hyperstretching leads to a significantly steeper increase and larger maximal value of the elongational stress growth coefficient than the assumption of affine stretch.
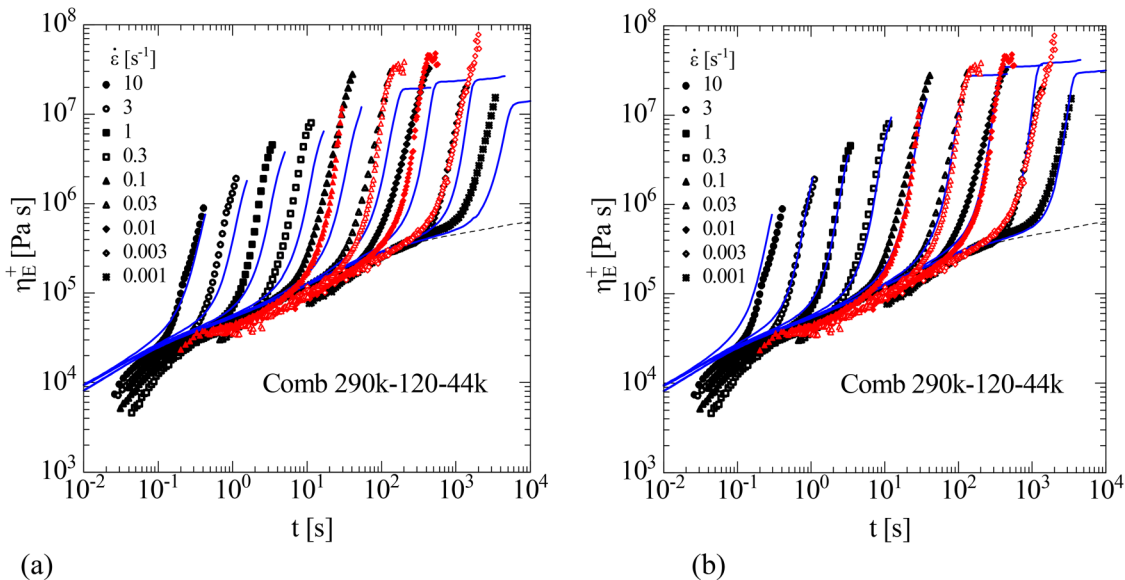

FIG. 8. Experimental data measured with EVF and FSR (black and more crowded symbols) of elongational stress growth coefficient $\eta_E^+(t)$ as a function of time t for the comb PS290k-60-44k at T = 180 °C. Lines are predictions of the HMMSF model with $k = 0$ (a) and $k = 0.6$ (b). $G_D = G_N^0 = 2.5 \times 10^5$ Pa.
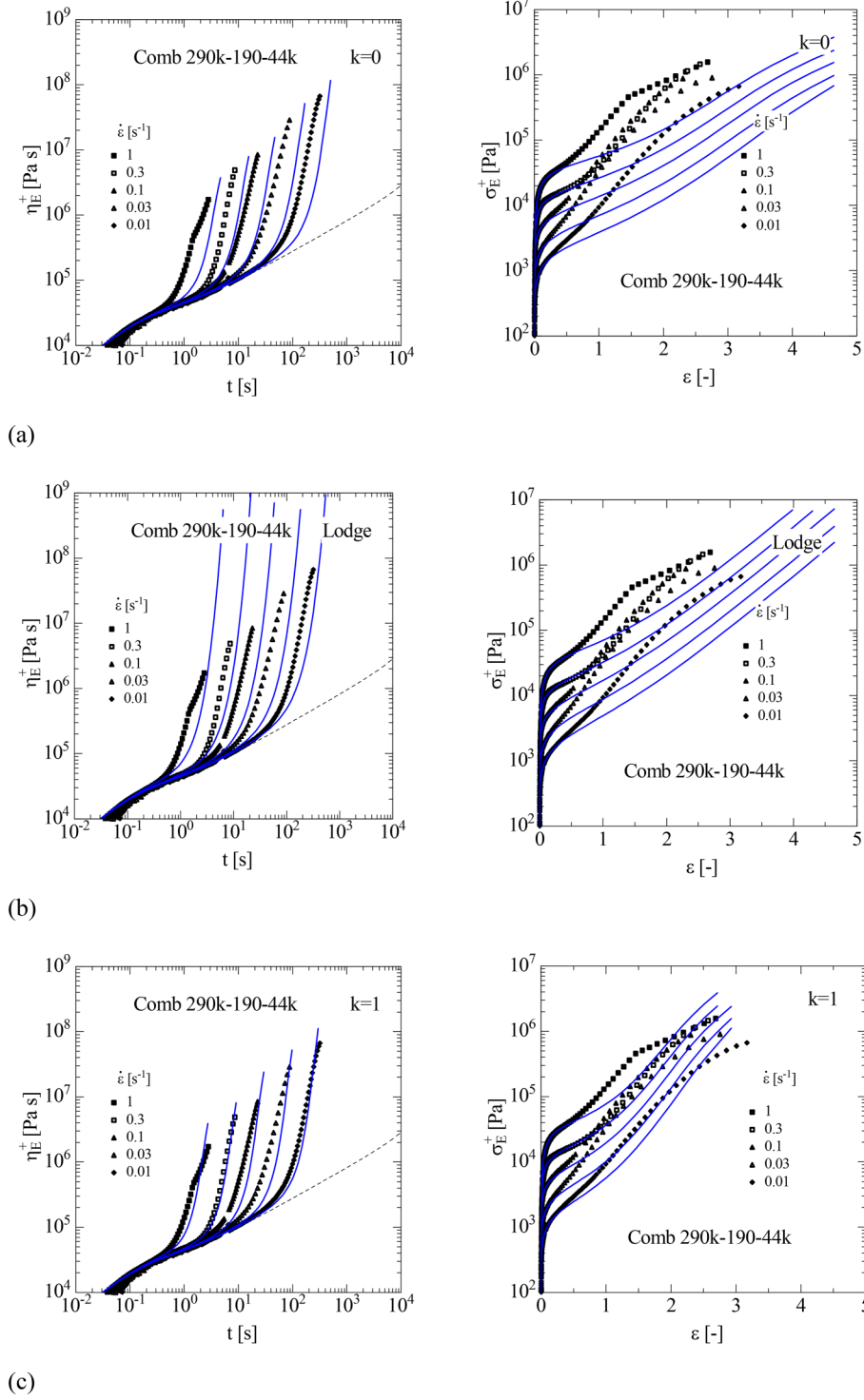
FIG. 9. Experimental data (symbols) of elongational stress growth coefficient $\eta_E^+(t)$ as a function of time t and elongational stress $\sigma_E^+(\varepsilon)$ as a function of Hencky strain ε for the comb PS290k-190-44k at T = 180 °C. Lines in (a) and (c) are predictions of the HMMSF model with $G_D = G_N^0 = 1.9 \times 10^5$ Pa and $k = 0$ (a), and $k = 1$ (c), respectively. Lines in (b) are predications of the Lodge rubberlike liquid, Eq. (15).

Figure 9 compares experimental data of elongational flow of comb PS290k-190-44k with 190 branches to predictions of the HMMSF model without hyperstretching ($k = 0$) and with maximal hyperstretching, i.e., $k = 1$. We recall from Eq. (10) that $k = 0$ corresponds to affine stretch in proportion to $\langle u' \rangle_0$, while the stretch increases with $\langle u' \rangle_0^2$ for $k = 1$. It is obvious that the elongational stress growth coefficient $\eta_E^+(t)$

exhibits a steeper slope, and the elongational stress growth $\sigma_E^+(\varepsilon)$, a stronger increase with the Hencky strain than expected for affine stretch, i.e., for $k = 0$ [Fig. 9(a)]. Also as shown in Fig. 9(b), the Lodge rubberlike liquid, Eq. (15), based on the assumption of affine deformation underpredicts the elongational stress growth data substantially. Although the experimental data show some scatter as most clearly seen
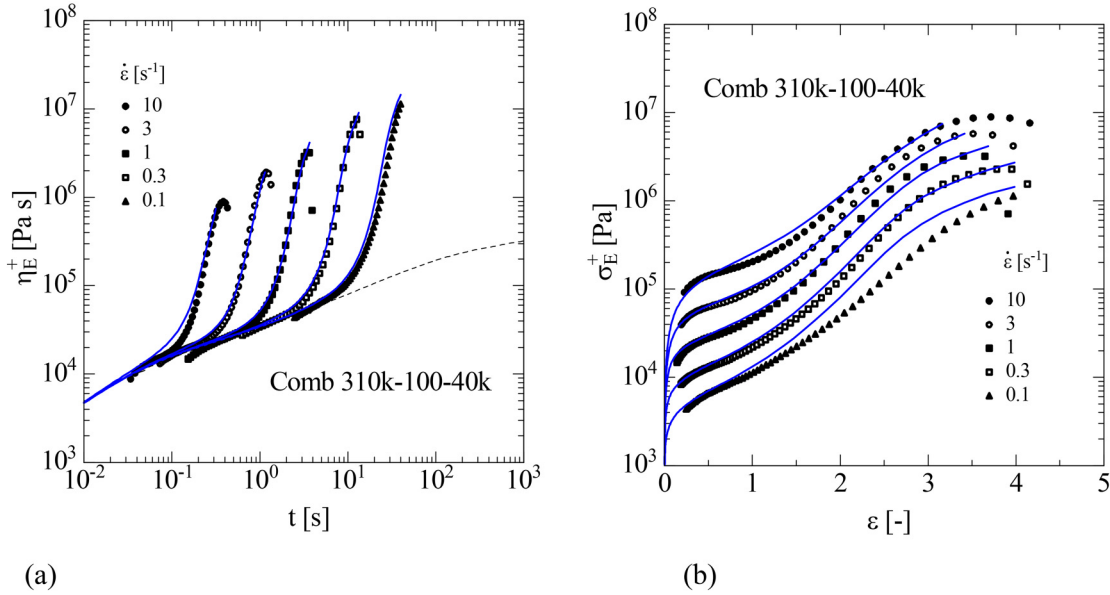
FIG. 10. Experimental data (symbols) of (a) elongational stress growth coefficient $\eta_E^+(t)$ as a function of time t and (b) elongational stress $\sigma_E^+(\varepsilon)$ as a function of Hencky strain ε for the comb PS310k-100-40k at T = 180 °C. Lines are predictions of the HMMSF model with $G_D = G_N^0 = 2.2 \times 10^5$ Pa and $k = 0.6$.

in the elongational stress growth data, general agreement of data and the HMMSF model is achieved by a hyperstretch parameter of $k = 1$ [Fig. 9(c)]. For 290k-190-44k, the number of branches per entanglement is $N_b \cong 10$, i.e., in each entanglement segment of the backbone with $M_e = 14.5$ kg/mol, there are, on average, 10 branches of $M_{w,br} \cong 44$ kg/mol. It is conceivable that this leads to maximal hyperstretching of the backbone. We also find that the fracture criterion according to Eq. (16) is in agreement with experimental data of $\sigma_E^+(\varepsilon)$, which show fracture at Hencky strains of $\varepsilon \leq 3$.

The results obtained for the comb systems PS290-Nbr-44k are supported by elongational measurements of comb PS310k-100-40k [27] with backbone $M_{w,bb}$ = 310 kg/mol and 100 branches of molecular weight $M_{w,br}$ $\cong 40$ kg/mol. Agreement between experimental data of the elongational stress growth coefficient $\eta_E^+(t)$ and the elongational stress $\sigma_E^+(\varepsilon)$ with predictions of the HMMSF model is obtained by a hyperstretch factor of $k = 0.6$ (Fig. 10) This corresponds to the same hyperstretching as seen for comb PS290k-120-44k, which has $N_b \cong 6$ branches per entanglement segment of the backbone, while the comb PS310k-100-40k has $N_b \cong 5$. The dilution modulus G_D of comb PS310k-100-40k is again identical to the plateau modulus G_N^0, as in the case of the densely grafted comb polymers of PS290-Nbr-44k with Nbr ≥ 30 and $N_b > 1$.

We finally note that there is a remarkable qualitative difference between the elongational behavior of densely grafted combs with $N_b > 1$ and so-called pom-pom polymer melts. While the arms of combs are statistically distributed along the backbone, the branches of pom-poms are all located at either end of the backbone, i.e., a pom-poms may be considered as a comb with its branches placed each half of them at the two ends of the backbone. The PS pom-poms investigated in [43] have formal values of N_b between 0.7 and 6.5, if the number of backbone entanglements is divided by the total number of arms at both ends of the backbone. The

HMMSF model was found to describe well the elongational rheology of all 10 pom-poms investigated, independently of the value of N_b, by assuming affine stretch (i.e., $k = 0$) of the backbone and without any signature of hyperstretching effects. Thus, it is not only the average number of branches per entanglement that determines hyperstretching, but the exact location of the branches along the backbone. Only if there is more than one side chain within an actual entanglement segment, these side chains act as additional topological constraints or "subentanglements" on length scales smaller than the tube diameter and create the extra tension, which leads to hyperstretching.

V. COMPARISON OF ELONGATIONAL VISCOSITY DATA OF COMBS WITH BRANCH-ON-BRANCH TOPOLOGY TO MODEL PREDICTIONS

The comb PS310k-100-40k with 100 first-generation long-chain branches (lcbs) of $M_{w,lcb} = 40$ kg/mol served as the precursor for the synthesis of the dendrigraft-type branch-on-branch (BoB) structures by adding a second generation of 120 to 460 short-chain branches (scbs) with $M_{w,scb}$ $\cong 14$ kg/mol on the long-chain branches [27]. In Fig. 11, experimental data of the elongational stress growth coefficient $\eta_E^+(t)$ of the BoB 310k-100-40k-g-120-14k are compared with predictions of the HMMSF model without hyperstretching ($k = 0$) and maximal hyperstretching ($k = 1$). Again, the experimental data of elongational stress growth coefficient $\eta_E^+(t)$ and elongational stress growth $\sigma_E^+(\varepsilon)$ show a much stronger increase with time and Hencky strain than expected for affine stretch, i.e., for $k = 0$ [Fig. 11(a)]. In spite of some inconsistencies of the experimental data as clearly seen in the elongational stress growth $\sigma_E^+(\varepsilon)$, general agreement of data and the HMMSF model is achieved by a hyperstretch parameter of $k = 1$ [Fig. 11(b)]. The same result is obtained for BoB 310k-100-40k-g-240-14k and BoB
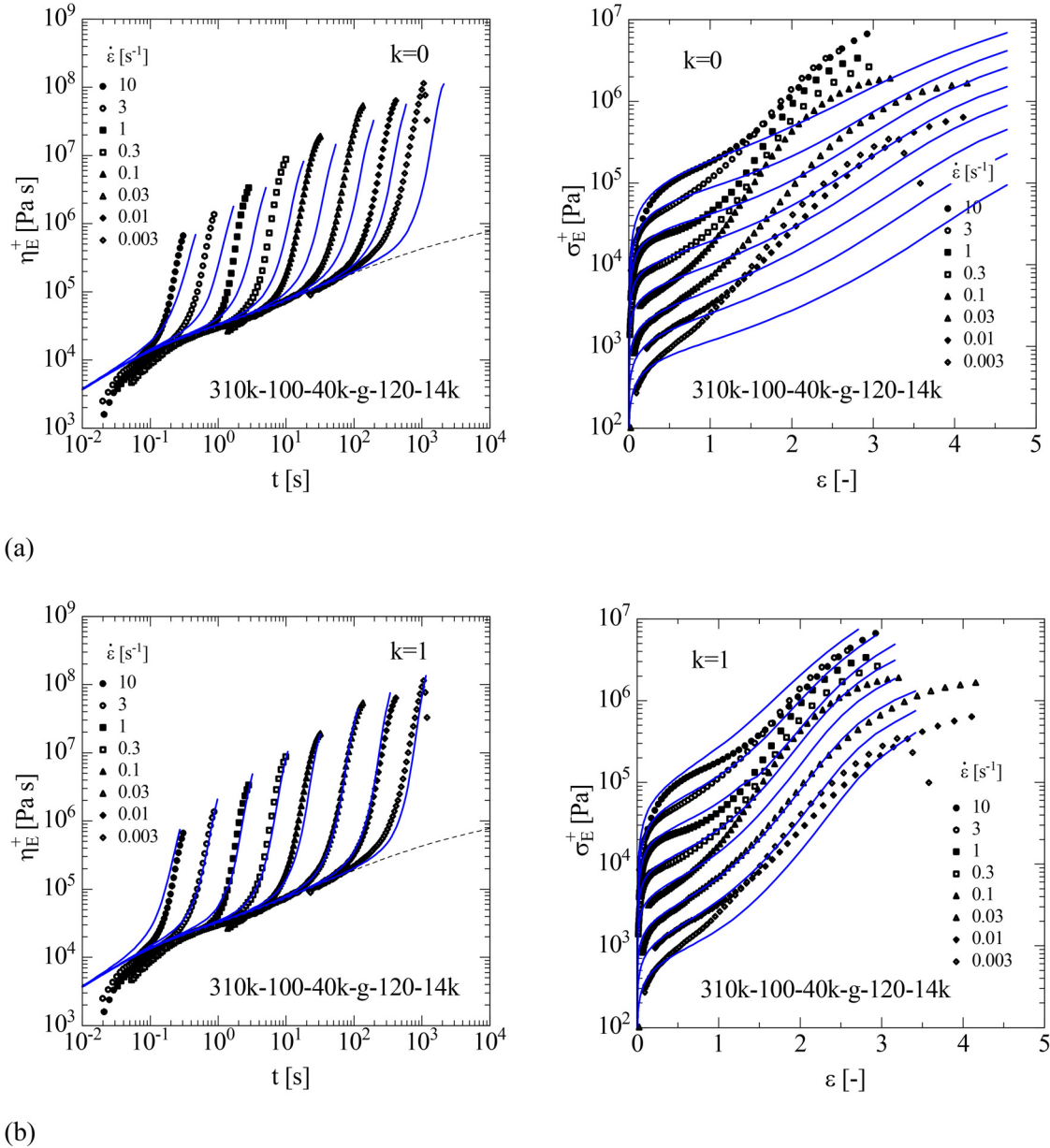
FIG. 11. Experimental data (symbols) of elongational stress growth coefficient $\eta_E^+(t)$ as a function of time t and elongational stress $\sigma_E^+(\varepsilon)$ as a function of Hencky strain ε for the BoB 310k-100-40k-g-120-14k at T = 180 °C. Lines are predictions of the HMMSF model with $G_D = G_N^0 = 2.2 \times 10^5$ Pa and $k = 0$ (a), and $k = 1$ (b), respectively.

310k-100-40k-g-460-13k (Fig. 12). The 120 to 460 short-chain branches grafted onto the 100 long-chain branches create substantial extra entanglements, which increase not only the relaxation times and the zero-shear viscosity of the BoB polymers (Table IV), but also lead to extremely high transient strain hardening with strain hardening factors of up to 600 [27] and maximal hyperstretching. This is caused by five BoB side chains per entanglement segment of the back-bone ($N_b \cong 5$) in combination with the 120 to 460 branch points on the BoB side chains, which leads to higher friction and extra tension. For BoB 310k-100-40k-g-460-13k, agreement of experimental data and predictions of the HMMSF model is found at higher strain rates, while at lower strain rates, there are some deviations between the experiment and the model.

VI. MODELING ELONGATIONAL VISCOSITY OF COMB/LINEAR BLENDS

The results obtained for the comb system PS290-Nbr-44k are further supported by elongational measurements at 160 °C of the comb PS310k-100-15k with backbone $M_{w,bb}$ = 310 kg/mol and 100 branches of molecular weight $M_{w,br} \cong 15$ kg/mol, respectively. Again, as in the case of the pure comb PS310k-100-40k, agreement between experimental data of the elongational stress growth coefficient $\eta_E^+(t)$ and the elongational stress $\sigma_E^+(\varepsilon)$ with predictions of the HMMSF model is obtained by a hyperstretch factor of $k = 0.6$ (Fig. 13). The molecular weight of the branches, $M_{w,br} \cong 15$ kg/mol versus $M_{w,br} \cong 40$ kg/mol, has seemingly no influence on hyperstretching as long as the branches are at least marginally entangled.
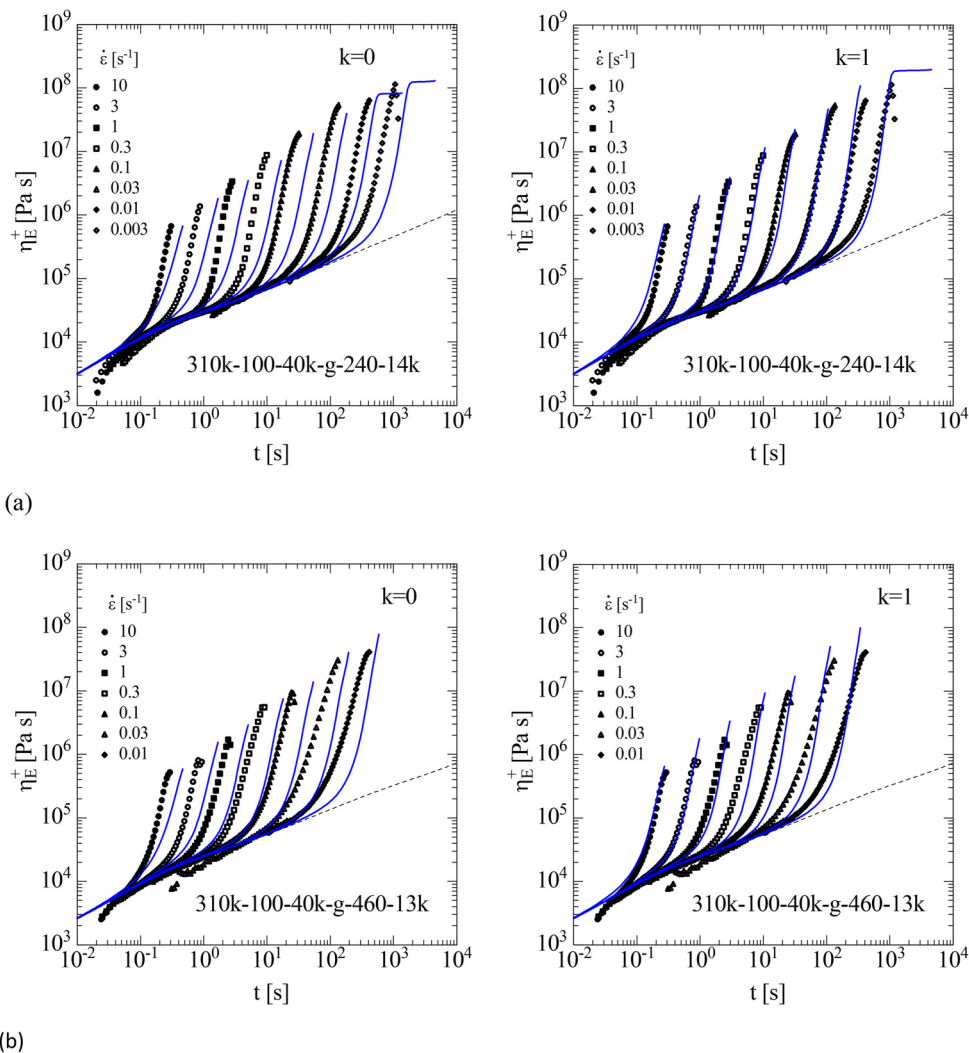
FIG. 12. Measurements (symbols) of elongational stress growth coefficient $\eta_E^+(t)$ as a function of time t for (a) BoB 310k-100-40k-g-240-14k and (b) BoB 310k-100-40k-g-460-13k at T = 180 °C. Lines are predictions of the HMMSF model with $k = 0$ and $k = 1$. $G_D = G_N^0$ as given in Table IV.
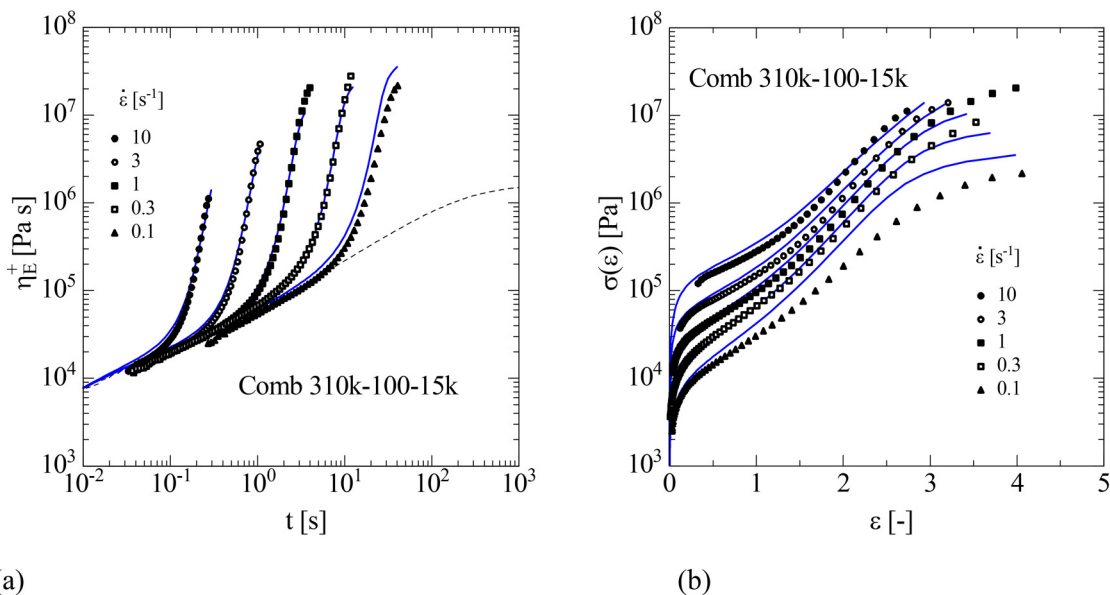

FIG. 13. Measurements (symbols) of (a) elongational stress growth coefficient $\eta_E^+(t)$ as a function of time t and (b) elongational stress $\sigma_E^+(\varepsilon)$ as a function of Hencky strain ε for the comb PS310k-100-15k at T = 160 °C. Lines are predictions of the HMMSF model with $G_D = G_N^0 = 3.2 \times 10^5$ Pa and $k = 0.6$.
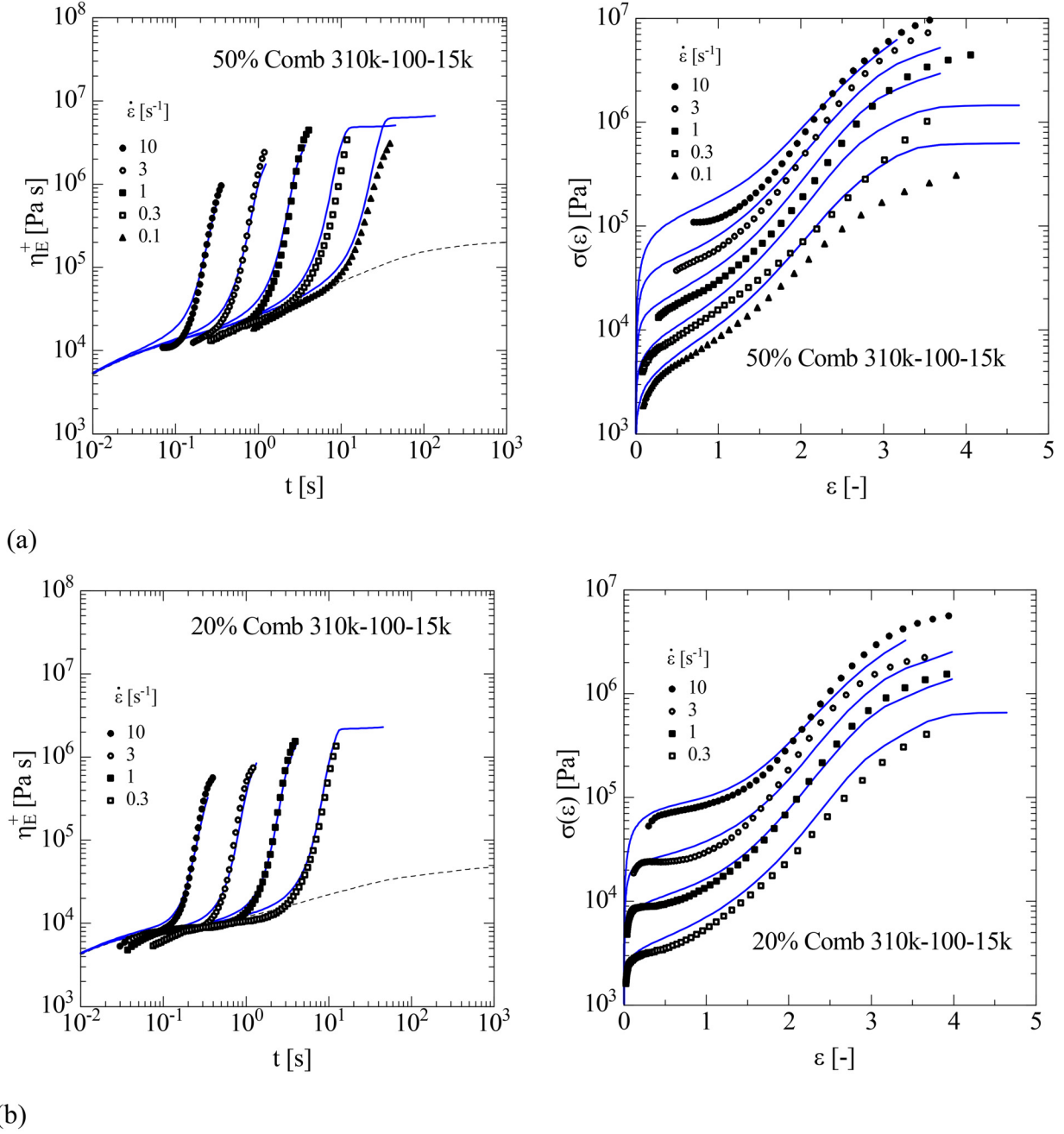
(a)

(b)

FIG. 14. Experimental data (symbols) of elongational stress growth coefficient $\eta_E^+(t)$ as a function of time t (left panels) and elongational stress $\sigma_E^+(\varepsilon)$ as a function of Hencky strain ε (right panels) for blends of the comb PS310k-100-15k (in wt. %) and linear PS43k at T = 160 °C. Lines are predictions of the HMMSF model with $k = 0.6$ and $G_D = G_N^0$ as given in Table IV.

Figure 14 shows measurements (symbols) of elongational stress growth coefficient $\eta_E^+(t)$ as a function of time t (left panels) and elongational stress growth $\sigma_E^+(\varepsilon)$ as a function of Hencky strain ε (right panels) for blends of the comb PS310k-100-15k and linear PS43k at T = 160 °C. We note that the Rouse time of PS43k at 160 °C can be estimated as 0.02 s [14], and thus at elongation rates $\dot{\varepsilon} \le 50\,\mathrm{s}^{-1}$, the PS43k chains will not be stretched but act simply as a diluent. Remarkably, with the same hyperstretch factor of $k = 0.6$ as for the neat comb PS310k-100-15k, and with dilution modulus G_D being identical to the plateau modulus, i.e., $G_D = G_N^0$ (Table III), agreement between experimental data

and the HMMSF model is obtained for all blends with 5–50 wt. % of comb PS310k-100-15k investigated. This shows that hyperstretching is an intrinsic property of the comb macromolecule with $N_b > 1$, independent of the comb concentration in the blend. From a practical point of view, adding even 5% of densely grafted comb structures with hyperstretching performance to a low-molecular-weight linear polymer results in significant SHF under extensional deformation. This can be used as a toolbox for polymer blends to adjust the melt rheological properties via low amount of hyperstretching polymers and keep the performance in solid mechanical properties through the molecular weight of the linear polymer.
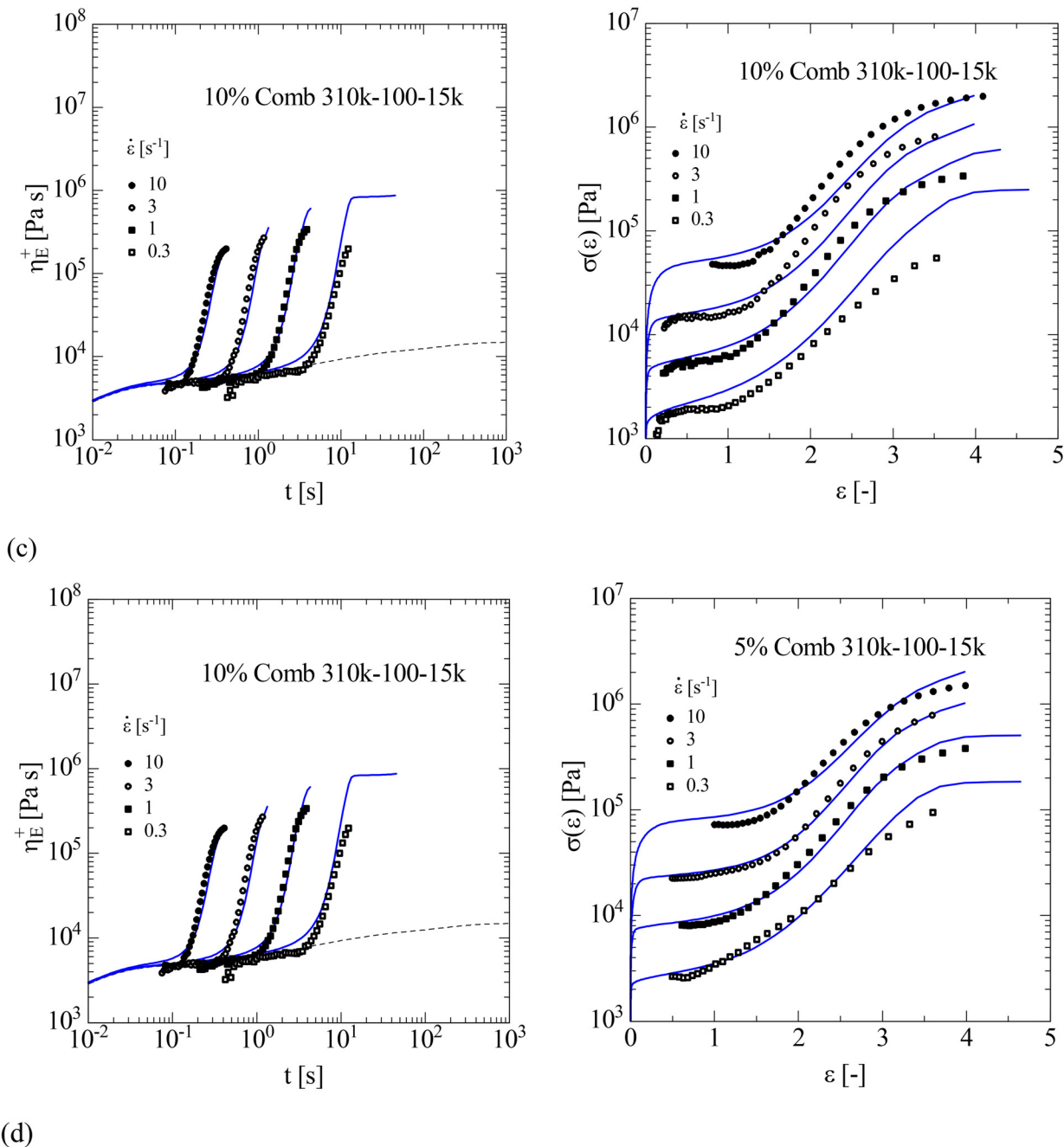
(c)

(d)

FIG. 14. (*Continued*)

VII. CONCLUSIONS

We have extended the hierarchical multimode molecular stress function (HMMSF) model to account for hyperstretching of densely grafted combs with $N_b > 1$ branches per entanglement segment of the backbone by introducing a hyperstretch factor k. While affine stretch leads to a reduction of the volume of tube segments with increasing deformation and is characterized by a hyperstretch factor of $k = 0$, maximal hyperstretching is characterized by a constant tube segment volume and a hyperstretch factor of $k = 1$. We considered the elongational flow data of the comb series PS290k-Nbr-44k with the number of branches Nbr ranging from 3 to 190 corresponding to an average number N_b of branches per entanglement segment of

the backbone from $N_b \cong 0.2$ to $N_b \cong 10$. A detailed analysis by the HMMSF model reveals that while backbone chains of loosely grafted combs with $N_b < 1$ are stretched affinely in elongational flow ($k = 0$), backbone chains of more densely grafted combs with $N_b > 1$ show increasing hyperstretching with increasing N_b, which can be quantified by hyperstretch factors $0 < k \leq 1$. Maximal hyperstretch is found for comb PS290k-190-44k with 190 branches and $N_b \cong 10$ with $k = 1$. We may conclude that in loosely grafted combs with $N_b < 1$, branch points and entanglements pin the backbone chain to the deforming continuum of the surrounding chains, leading to affine stretch of entanglement segments of the backbone, while in densely grafted combs with $N_b > 1$, the additional branch points within an entanglement segment create additional

tension in the backbone, i.e., lead to hyperstretching. In contrast, pom-pom melts with the branches placed exactly at the two ends of the backbone do not show hyperstretching in elongation, even if formally, the value of N_b of branches per entanglement segment of the backbone is larger than one.

These results are supported by the analysis of elongational flow measurements of comb PS310-100-40 k with backbone $M_{w,bb} = 310$ kg/mol and 100 branches of $M_{w,br} \cong 40$ kg/mol, and a similar comb with shorter but still entangled branches, i.e., PS310-100-15k with branches of molecular weight $M_{w,br} \cong 15$ kg/mol. Excellent agreement of experimental data and HMMSF model predictions is obtained by a hyperstretch factor of $k = 0.6$. The same amount of hyperstretching is seen for comb PS290k-120-44k with $N_b \cong 6$ branches per entanglement segment of the backbone, while 310k-100-15k has $N_b \cong 5$. It seems that in the range of $M_{w,br}$ from 15 to 40 kg/mol, hyperstretching is predominantly caused by the number N_b of branches rather than their length, at least as long as the branches have a molecular weight $M_{w,br}$ equal or larger than the entanglement molecular weight M_e. On the other hand, the dendrigraft-type branch-on-branch (BoB) polymers with 120 to 460 scb with $M_{w,scb} \cong 14$ kg/mol grafted onto the 100 long-chain branches of $M_{w,br} \cong 40$ kg/mol display maximal hyperstretching ($k = 1$). This is caused by the branch points on the BoB side chains, leading to additional friction and increasing the tension in the backbone.

Remarkably, the same amount of hyperstretching with $k = 0.6$ as for the pure PS310-100-15k is also found in blends of 5–50 wt. % of comb PS310k-100-15k and linear PS43k. This shows that hyperstretching is an intrinsic property of the comb macromolecule with $N_b > 1$, independent of its concentration in the blend. Hyperstretching can have a significant impact on the processability of polymer melts, and the quantification of this effect is, therefore, important.

The HMMSF model is based on the concepts of hierarchical relaxation and dynamic dilution. Dynamic dilution of chain segments with longer relaxation times by chain segments with shorter relaxation times starts as soon as the relaxation process has reached the dilution modulus $G_D \le G_N^0$. In general, the dilution modulus G_D is a free parameter of the constitutive model, which needs to be fitted to nonlinear viscoelastic experimental evidence. However, for the comb systems PS290k-Nbr-44k with Nbr ≥ 30 as well as for PS310k-100-15k, PS310-100-40k, and the BoB polymers based on PS310-100-40k, dynamic dilution of the backbone starts as soon as the relaxation modulus $G(t)$ has reached the value of the plateau modulus. For the well-defined combs investigated with $N_b > 1$, the dilution modulus G_D is identical to the plateau modulus G_N^0 of the polymer. This is even true for the blends of 5–50 wt. % of comb PS310k-100-44k and linear PS43k, for which the assumption of the dilution modulus G_D being identical to the plateau modulus, i.e., $G_D = G_N^0$, leads to excellent agreement between experimental data and the HMMSF model for all blends investigated.

ACKNOWLEDGMENTS

AUTHOR DECLARATIONS

Conflict of Interest

REFERENCES

[1] Geyer, R., Production, use, and fate of synthetic polymers, in *Plastic Waste and Recycling* (Elsevier, San Diego, 2020), pp. 13–32. .

[2] Larson, R. G., *The Structure and Rheology of Complex Fluids* (Oxford University, 1999).

[3] McLeish, T. C. B., and R. G. Larson, "Molecular constitutive equations for a class of branched polymers: The pom-pom polymer," J. Rheol. **42**(1), 81–110 (1998).

[4] Dealy, J. M., and R. G. Larson, *Structure and Rheology of Molten Polymers: From Structure to Flow Behavior and Back Again* (Hanser, München, 2006).

[5] Münstedt, H., "Various features of melt strain hardening of polymeric materials in uniaxial extension and their relation to molecular structure: Review of experimental results and their interpretation," Rheol. Acta **62**(7-8), 333–363 (2023).

[6] Huang, Q., "When polymer chains are highly aligned: A perspective on extensional rheology," Macromolecules **55**(3), 715–727 (2022).

[7] Matsumiya, Y., and H. Watanabe, "Non-universal features in uniaxially extensional rheology of linear polymer melts and concentrated solutions: A review," Prog. Polym. Sci. **112**, 101325 (2021).

[8] McLeish, T. C. B., "Tube theory of entangled polymer dynamics," Adv. Phys. **51**(6), 1379–1527 (2002).

[9] McLeish, T. C. B., J. Allgaier, D. K. Bick, G. Bishko, P. Biswas, R. Blackwell, B. Blottière, N. Clarke, B. Gibbs, D. J. Groves, A. Hakiki, R. K. Heenan, J. M. Johnson, R. Kant, D. J. Read, and R. N. Young, "Dynamics of entangled H-polymers: Theory, rheology, and neutron-scattering," Macromolecules **32**(20), 6734–6758 (1999).

[10] Stadler, F. J., J. Kaschta, H. Münstedt, F. Becker, and M. Buback, "Influence of molar mass distribution and long-chain branching on strain hardening of low density polyethylene," Rheol. Acta **48**, 479–490 (2009).

[11] Frischknecht, A. L., S. T. Milner, A. Pryke, R. N. Young, R. Hawkins, and T. C. B. McLeish, "Rheology of three-arm asymmetric star polymer melts," Macromolecules **35**(12), 4801–4820 (2002).

[12] Graessley, W. W., and J. Roovers, "Melt rheology of four-arm and six-arm star polystyrenes," Macromolecules **12**(5), 959–965 (1979).

[13] Abbasi, M., L. Faust, K. Riazi, and M. Wilhelm, "Linear and extensional rheology of model branched polystyrenes: From loosely grafted combs to bottlebrushes," Macromolecules **50**(15), 5964–5977 (2017).

[14] Lentzakis, H., D. Vlassopoulos, D. J. Read, H. Lee, T. Chang, P. Driva, and N. Hadjichristidis, "Uniaxial extensional rheology of well-characterized comb polymers," J. Rheol. **57**(2), 605–625 (2013).

[15] Kapnistos, M., D. Vlassopoulos, J. Roovers, and L. G. Leal, "Linear rheology of architecturally complex macromolecules: Comb polymers with linear backbones," Macromolecules **38**(18), 7852–7862 (2005).

[16] Lentzakis, H., C. Das, D. Vlassopoulos, and D. J. Read, "Pom-pom-like constitutive equations for comb polymers," J. Rheol. **58**(6), 1855–1875 (2014).

[17] Roovers, J., and W. W. Graessley, "Melt rheology of some model comb polystyrenes," Macromolecules **14**(3), 766–773 (1981).

[18] López-Barrón, C. R., and M. E. Shivokhin, "Extensional strain hardening in highly entangled molecular bottlebrushes," Phys. Rev. Lett. **122**(3), 37801 (2019).

[19] López-Barrón, C. R., M. E. Shivokhin, and J. R. Hagadorn, "Extensional rheology of highly-entangled α-olefin molecular bottlebrushes," J. Rheol. **63**(6), 917–926 (2019).

[20] Zografos, A., H. A. All, A. B. Chang, M. A. Hillmyer, and F. S. Bates, "Star-to-Bottlebrush transition in extensional and shear deformation of unentangled polymer melts," Macromolecules **56**(6), 2406–2417 (2023).

[21] Ianniello, V., and S. Costanzo, "Linear and nonlinear shear rheology of nearly unentangled H-polymer melts and solutions," Rheol. Acta **61**(10), 667–679 (2022).

[22] Nielsen, J. K., H. K. Rasmussen, M. Denberg, K. Almdal, and O. Hassager, "Nonlinear branch-point dynamics of multiarm polystyrene," Macromolecules **39**(25), 8844–8853 (2006).

[23] Houli, S., H. Iatrou, N. Hadjichristidis, and D. Vlassopoulos, "Synthesis and viscoelastic properties of model dumbbell copolymers consisting of a polystyrene connector and two 32-arm star polybutadienes," Macromolecules **35**(17), 6592–6597 (2002).

[24] Röpert, M.-C., M. G. Schußmann, M. K. Esfahani, M. Wilhelm, and V. Hirschberg, "Effect of side chain length in polystyrene POM–POMs on melt rheology and solid mechanical fatigue," Macromolecules **55**, 5485–5496 (2022).

[25] Röpert, M.-C., A. Goecke, M. Wilhelm, and V. Hirschberg, "Threading polystyrene stars: Impact of star to POM-POM and barbwire topology on melt rheological and foaming properties," Macromol. Chem. Phys. **223**, 2200288 (2022).

[26] van Ruymbeke, E., M. Kapnistos, D. Vlassopoulos, T. Huang, and D. M. Knauss, "Linear melt rheology of Pom-Pom polystyrenes with unentangled branches," Macromolecules **40**(5), 1713–1719 (2007).

[27] Faust, L., M.-C. Röpert, M. K. Esfahani, M. Abbasi, V. Hirschberg, and M. Wilhelm, "Comb and branch-on-branch model polystyrenes with exceptionally high strain hardening factor SHF > 1000 and their impact on physical foaming," Macromol. Chem. Phys. **224**(1), 2200214 (2023).

[28] van Ruymbeke, E., E. B. Muliawan, S. G. Hatzikiriakos, T. Watanabe, A. Hirao, and D. Vlassopoulos, "Viscoelasticity and extensional rheology of model Cayley-tree polymers of different generations," J. Rheol. **54**(3), 643–662 (2010).

[29] Larson, R. G., "Combinatorial rheology of branched polymer melts," Macromolecules **34**(13), 4556–4571 (2001).

[30] Borger, A., W. Wang, T. C. O'Connor, T. Ge, G. S. Grest, G. V. Jensen, J. Ahn, T. Chang, O. Hassager, K. Mortensen, D. Vlassopoulos, and Q. Huang, "Threading-unthreading transition of linear-ring polymer blends in extensional flow," ACS Macro Lett. **9**(10), 1452–1457 (2020).

[31] Ebrahimi, T., H. Taghipour, D. Grießl, P. Mehrkhodavandi, S. G. Hatzikiriakos, and E. van Ruymbeke, "Binary blends of entangled star and linear poly(hydroxybutyrate): Effect of constraint release and dynamic tube dilation," Macromolecules **50**(6), 2535–2546 (2017).

[32] Hirschberg, V., S. Lyu, M. G. Schußmann, M. Wilhelm, and M. H. Wagner, "Modeling elongational viscosity of polystyrene Pom-Pom/linear and Pom-Pom/star blends," Rheol. Acta **62**, 433–445 (2023).

[33] Yan, Z.-C., E. van Ruymbeke, and D. Vlassopoulos, "Linear viscoelastic response of comb/linear polymer blends: A three-step relaxation process," Macromolecules **54**(23), 11047–11060 (2021).

[34] Zhou, Y., C. D. Young, M. Lee, S. Banik, D. Kong, G. B. McKenna, R. M. Robertson-Anderson, C. E. Sing, and C. M. Schroeder, "Dynamics and rheology of ring-linear blend semidilute solutions in extensional flow: Single molecule experiments," J. Rheol. **65**(4), 729–744 (2021).

[35] Doi, M., and S. F. Edwards, "Dynamics of concentrated polymer systems. Part 3.—The constitutive equation," J. Chem. Soc., Faraday Trans. 2 **74**, 1818–1832 (1978).

[36] Doi, M., and S. F. Edwards, "Dynamics of concentrated polymer systems. Part 4.—Rheological properties," J. Chem. Soc., Faraday Trans. 2 **75**, 38–54 (1979).

[37] Dealy, J. M., D. J. Read, and R. G. Larson, *Structure and Rheology of Molten Polymers: From Structure to Flow Behavior and Back Again*, 2nd ed. (Hanser, München, 2018).

[38] Narimissa, E., and M. H. Wagner, "Review on tube model based constitutive equations for polydisperse linear and long-chain branched polymer melts," J. Rheol. **63**(2), 361–375 (2019).

[39] Wagner, M. H., P. Rubio, and H. Bastian, "The molecular stress function model for polydisperse polymer melts with dissipative convective constraint release," J. Rheol. **45**(6), 1387–1412 (2001).

[40] Narimissa, E., and M. H. Wagner, "From linear viscoelasticity to elongational flow of polydisperse linear and branched polymer melts: The hierarchical multi-mode molecular stress function model," Polymer **104**, 204–214 (2016).

[41] Narimissa, E., and M. H. Wagner, "A hierarchical multimode molecular stress function model for linear polymer melts in extensional flows," J. Rheol. **60**(4), 625–636 (2016).

[42] Wagner, M. H., E. Narimissa, L. Poh, and Q. Huang, "Modelling elongational viscosity overshoot and brittle fracture of low-density polyethylene melts," Rheol. Acta **61**(4–5), 281–298 (2022).

[43] Hirschberg, V., M. G. Schußmann, M.-C. Röpert, M. Wilhelm, and M. H. Wagner, "Modeling elongational viscosity and brittle fracture of 10 polystyrene Pom-poms by the hierarchical molecular stress function model," Rheol. Acta **62**, 269–283 (2023).

[44] Huang, Q., and O. Hassager, "Polymer liquids fracture like solids," Soft matter **13**(19), 3470–3474 (2017).

[45] Huang, Q., N. J. Alvarez, A. Shabbir, and O. Hassager, "Multiple cracks propagate simultaneously in polymer liquids in tension," Phys. Rev. Lett. **117**(8), 87801 (2016).

[46] Wagner, M. H., E. Narimissa, and Q. Huang, "Scaling relations for brittle fracture of entangled polystyrene melts and solutions in elongational flow," J. Rheol. **65**(31), 311–324 (2021).

[47] Wagner, M. H., and V. Hirschberg, "Experimental validation of the hierarchical multi-mode molecular stress function model in elongational flow of long-chain branched polymer melts," J. Non-Newton. Fluid Mech. **321**, 105130 (2023).

[48] Narimissa, E., V. H. Rolón-Garrido, and M. H. Wagner, "A hierarchical multi-mode MSF model for long-chain branched polymer melts part I: Elongational flow," Rheol. Acta **54**(9–10), 779–791 (2015).

[49] Kempf, M., D. Ahirwal, M. Cziep, and M. Wilhelm, "Synthesis and linear and nonlinear melt rheology of well-defined comb architectures of PS and PpMS with a low and controlled degree of long-chain branching," Macromolecules **46**(12), 4978–4994 (2013).

[50] Shahid, T., C. Clasen, F. Oosterlinck, and E. van Ruymbeke, "Diluting entangled polymers affects transient hardening but not their steady elongational viscosity," Macromolecules **52**(6), 2521–2530 (2019).

[51] Huang, Q., M. Mangnus, N. J. Alvarez, R. Koopmans, and O. Hassager, "A new look at extensional rheology of low-density polyethylene," Rheol. Acta **55**(5), 343–350 (2016).

[52] Poh, L., E. Narimissa, M. H. Wagner, and H. H. Winter, "Interactive shear and extensional rheology—25 years of IRIS software," Rheol. Acta **61**(4-5), 259–269 (2022).

[53] Winter, H. H., and M. Mours, "The cyber infrastructure initiative for rheology," Rheol. Acta **45**(4), 331–338 (2006).

[54] See supplementary material online for figures of the mastercurves of G′, G″, tan δ; the TTS factors; as well as the Maxwell modes of all polymers investigated.